Perovskite Nanoparticles: Synthesis, Properties, and Novel Applications in Photovoltaics and LEDs

Sneha A. Kulkarni, Subodh G. Mhaisalkar, Nripan Mathews, and Pablo P. Boix**

Solar cells and light-emitting diodes (LEDs) based on metal-halide perovskites are transitioning from promising performers to direct competetors to well-established technologies, with cost-effectiveness as a strong advantage. Nanostructured perovskites have yielded record LEDs due to their higher versatility in the local management of charge carriers, which has enabled photoluminescence quantum yields (PLQYs) close to 100%.

However, these perovskite nanostructures are yet to be fully exploited in other applications such as photovoltaics, where they can also present competitive advantages as they enable feasible routes to surpass the Shockley–Queisser limit by means of multiexciton generation or hot-carrier extraction. Besides conventional applications, the extraordinary properties of these materials have the potential to unlock novel areas of research. Herein, the potential of perovskite nanostructures—with the focus on the widely developed nanoparticles—beyond classical thin-film optoelectronics is analyzed, their limits of application are discussed, and their real possibilities are pondered.

1. Introduction

Halide perovskites have attracted the noticeable attention of the optoelectronic community due to their exceptional optical and electronic properties; include long charge carrier diffusion lengths, sharp absorption edges with small Urbach tails, bandgap tunability over visible range, easy and cost-effective solution processability.[1–4] These qualities, signs of benign structural defects, have resulted in perovskite solar cells with performances approaching those of more expensively processed inorganic materials, as well as extremely promising light-emitting diodes.[5–11] Their optical and electronic properties can be tuned by varying the compositions of metal ion (Pb^{2+}, Sn^{2+}, Ge^{2+}), cation [methylammonium ($CH_3NH_3^+$ = MA^+) or formamidinium ($HC(NH_2)_2^+$ = FA^+), Cs^+], as well as anion (Cl^-, I^-, Br^-, or a mixture halide), which usually form a 3D structural framework of the AMX_3- type (**Figure 1**A). In addition, the size, shape, and structural dimensionality of perovskite nanostructure can be regulated with systematic variation of the ratio between the long chain amine ligand and perovskite precursor[12–14] (Figure 1). They exhibit shape- and size-dependent optical and electronic properties distinct from their bulk counterparts due to quantum confinement or strong anisotropy. Perovskite "quantum dots" (QDs) assume a dimension smaller than the exciton Bohr radius. Generally, perovskite nanostructures display higher photoluminescence quantum yield (PLQY), particularly in suspension, which is probably related to the charge confinement and the lower defect concentration. Nevertheless, their charge transport properties usually lay below those of 3D bulk perovskites. [13] Here, we have predominantly utilized "nanoparticle" as the term encompassing "nanocrystals" and "quantum dots" and have utilized nanostructures to refer to nanoplatelets, nanorods, nanowires, etc, for simplicity. Some distinct properties of the perovskite nanostructures as compared its bulk counterpart are summarized in **Figure 2**.[14–17] When the nanostructures, in this case nanoplatelets, are surrounded by an organic medium with a smaller dielectric constant, the screening of the electron–hole Coulomb interaction is less effective. It increases the exciton binding energy (E_b in the range 200–500 meV) of perovskite nanoplatelets by an order of magnitude as compared to the bulk phase (E_b in the range 5–60 meV). The higher E_b significantly reduces the exciton dissociation probability prior to radiative decay as compared to the bulk, resulting in superior PLQY.[15] For example, the measured exciton binding energies for $MAPbBr_3$ bulk and nanoparticles (NPs) are 84 and 320 meV, respectively (Figure 2B-a,b). The evolution of the PLQY values of perovskite materials in the bulk film and NPs are summarized in detail in our previous report.[18] It clearly indicates the higher PLQY for the perov- skite nanoparticles as compared to the bulk film. In addition, the perovskite NPs possess the peculiar electronic band structure as shown in Figure 2C, where defect states appear inside

Dr. S. A. Kulkarni, Prof. S. G. Mhaisalkar, Prof. N. Mathews
Energy Research Institute at Nanyang Technological University (ERI@N)
Research Techno Plaza, X-Frontier Bloc, Level 5, 50 Nanyang Drive
Singapore 637553, Singapore
E-mail: sakulkarni@ntu.edu.sg
Prof. S. G. Mhaisalkar, Prof. N. Mathews
School of Materials Science and Engineering
Nanyang Technological University
Nanyang Avenue, Singapore 639798, Singapore
Dr. P. P. Boix
Instituto de Ciencia Molecular
Universidad de Valencia
C/J. Beltrán 2, 46980 Paterna, Spain
E-mail: pablo.p.boix@uv.es

the bands and do not act as trap states. Hence, perovskite NPs possess higher PL properties over the conventional semiconductor NPs, which usually require electronic passivation layer of wider-gap semiconductors to achieve higher PL.[16] The QDs exhibit the size-dependent color tuning properties like inorganic QDs, while perovskite colloidal nanocrystals (NCs) exhibit the size-independent emission wavelength and of very high color purity, due to crystal structure–dependent electronic band structure (Figure 2D).[17]

The perovskite unit cell structure is very sensitive to the size of the "A" cation, and the addition of slightly larger cation can lead to reconstruction of the 3D framework to perovskites with reduced dimensionality.[19] For instance, larger "A" can form the 2D halide perovskites of A_2MX_4-type, comprising monomolecular layer of [MX_6] octahedral separated by "A" cation barrier layers, 1D A_3MX_5-type chain-like structure or A_4MX_6-type 0D structure.[19] While quasifree charge carriers can be more prominent in the metal-halide perovskite 3D structures, excitons are usually more confined in the 2D inorganic layers due to larger E_b.[20]

Quasi-2D perovskites can form multiple quantum wells (MQWs) of $A_2(AMX_3)_{n-1}MX_4$ structure, also known as Ruddlesden–Popper perovskites.[19] These are a combination of the AMX_3 (3D)- and A_2MX_4 (2D)-types where the inorganic layers usually act like quantum wells, whereas the organic layers adopt the role of barrier. The photoinduced charge carriers form excitons that can be effectively confined within the inorganic wells, and that confinement effect increases with decreasing well width, i.e., number of inorganic layers. Thus, the excitonic properties of the quasi-2D MQW can be systematically tailored from 3D to 2D by decreasing the inorganic layer number from $n = \infty$ to $n = 1$. These additional degrees of freedom introduced by 2D and quasi-2D perovskites can be used as an effective way to increase radiative efficiency, however lower dimensionality perovskites usually suffer from directional charge transport. This can become a problem to extract (or inject) charge perpendicularly to the layers' plane, and strategies such as nanostructuring the platelets have been proposed.[21]

In this review, we have discussed the characteristic optical properties of NP perovskites, as well as summarized their various synthesis methods. In addition, we review and ana- lyze the prospective of these perovskite nanoparticles beyond classical thin-film optoelectronics. We discuss their limits of application and ponder their real possibilities, considering their high PLQY as one of the main arguments to approach the Shockley–Queisser limit (SQL), which determines the maximum performance of single junction solar cells and light-emitting diodes as their reciprocal process.[22] Finally, we also examine their use in approaches to potentially overcome the limit.

2. Properties of Perovskites

Perovskite NPs offer additional degrees of freedom over the bulk films to control the optoelectrical properties. In general, halide perovskites exhibit excellent color (bandgap) tunable emission over a wavelength range of 390–1050 nm with high color purity (narrow full-width at half maximum) and high PLQY.[23] One

Sneha A. Kulkarni received her Ph.D. in physical and materials chemistry from the National Chemical Laboratory (NCL), University of Pune, India. In 2011, she joined the Energy Research Institute@ NTU (ERIAN), Nanyang Technological University, where she is presently working as a Senior Research Scientist. Her research interests are synthesis and application of nanomaterials for energy harvesting and storage. Her current research is involved in synthesis, characterization, and device fabrication of novel hybrid perovskite materials in applications for solar cells as well as perovskite LEDs (PeLEDs). She also worked as a postdoctoral fellow in the National University of Singapore (NUS) from 2008 to 2011.

Nripan Mathews is an Assistant Professor at the School of Materials Science and Engineering at the Energy Research Institute@ NTU (ERIAN), Nanyang Technological University. He has worked on multiple material systems and explored the optical and transport properties within them. These material systems include perovskites, metal oxides, organic thin films, 1D nanostructures, and molecular crystals. The primary focus of his work has centered around the fabrication of novel and high-performance devices which exploit the unique property of each material set. He has focused on applying these novel materials in applications such as solar cells, light emitting diodes, thin film transistors, artificial synapses and photoelectrochemical systems.

Pablo P. Boix received his Ph.D. in nanoscience and nanotechnology from the Universitat Jaume I (2012, Castelló, Spain) with the focus on unveiling the physical processes governing sensitized and organic solar cells. In 2012, he joined the Energy Research Institute at the Nanyang Technological University (Singapore) to study lead halide perovskites for photovoltaic and light emission applications. He worked on industrial development of perovskite solar cells (Dyesol Ltd., Lausanne, Switzerland) and, after that, he joined ICMol (Universitat de València) as a Ramon y Cajal fellow. His research has contributed to the implementation of new materials and device concepts.

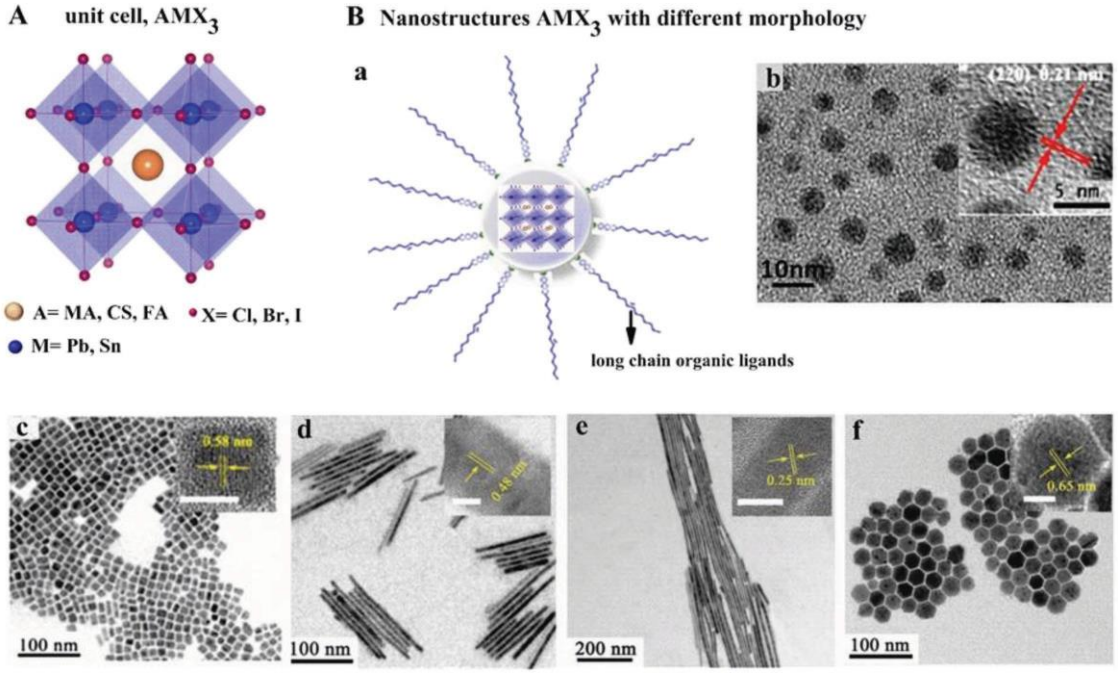

Figure 1. A) Representation of a perovskite unit cell and typical constituent ions. Adapted with permission.[14] Copyright 2017, American Chemical Society. B-a) Schematic illustration of a perovskite nanoparticle stabilized by oleate as surface ligands; B-b) typical TEM image and high-resolution TEM (HRTEM) image of perovskite nanoparticles of sample P-Br-5., i.e., $MAPbBr_3$ nanoparticles. Adapted with permission.[12] Copyright 2016, Nature Publishing Group. TEM images of the $CsPbX_3$ perovskite nanostructures with different morphologies: B-c) $CsPbBr_3$ nanocubes, B-d) $CsPbI_3$ nanorods, B-e) nanowires, and B-f) hexagonal nanoplates. Insets show the corresponding HRTEM images. Adapted with permission.[13] Copyright 2017, the Royal Society of Chemistry.

possibility to tune the bandgap of the perovskites over entire visible range is by chemically managing the composition of halide substituents, X, in AMX_3-type perovskites.[24] These modifications also have strong influences on the electronic energies and effective exciton mass.[25,26] However, the mixed halide approach sometimes induces phase segregation in the presence of light, adversely affecting the operation and reliability of optoelectronic devices. This instability arises from halide migration under continuous light illumination, which results in phase segregation and formation of traps or domains of the corresponding pure halides.[27] Similarly, the total or partial substitution of the metal cation directly modifies the resulting material's bandgap as well.[28] The σ antibonding orbitals of "B" cation (Pb 6s,) and halide ion (I 5p) are main contributors for valence band maximum (VBM) and π antibonding orbitals (Pb 6p, I 5p) for conduction band minimum. Nevertheless, the change in the "A" cation (for instance, with MA to FA) also alters the bandgap[29] due enhanced effect of hydrogen bonding between the cation and the inorganic octahedral network, resulting in the modification of the ionic/covalent character of the Pb□X bond.[27,30–34]

Besides 3D hybrid perovskites, tunable light emission in 2D layered and perovskite NPs has been demonstrated by controlling the size and shape[19,35–38] (**Figure 3**). These systems do not only offer excellent PLQY and stability, but also show the potential to overcome the issues related to ion migration and phase segregation, a clear advantage over the bulk thin films.[39–41] Quantum confinement effects start to influence the excitonic wave function when at least one of the physical dimensions approach the exciton Bohr radius of the material. Quantum confinement energy in semiconductor nanoparticles is indeed, calculated using effective mass approximation, with equation $\otimes E = \hbar^2\pi^2/2m^*r^2$, where m^* is the reduced mass of excitons and "r" is the particle radius.[37] According to the above equation, increment in confinement energy (ΔE) (i.e., blueshift in the resultant emission) could be achieved upon reduction in size (r) and exciton mass of the NPs (m^*).

For instance, the combination of halide compositional modulations as well as quantum size effects have been demonstrated to synthesize the $CsPbX_3$ NPs to attain an emission over an entire visible spectral region of 410–700 nm, i.e., wide color gamut covering up to 140% of the National Television System Committee (NTSC) color standard (Figure 3A).[37,42] In addition, $CsPbX_3$ NPs have shown the remarkably high PLQY of 50–90% and narrow emission (12–42 nm). The blueshift (from 512 to 460 nm) in the $CsPbBr_3$ NPs was noted with the size reduction from 11.8 to 3.8 nm (Figure 3B).[37] Similarly, the control of the particle size by means of a template method has been successfully employed to tune the emission of $CH_3NH_3PbBr_3$ NPs from ≈780 to ≈650 nm by controlling a particle size from ≈8 to 3 nm.[43]

The same routes employed to modify the bandgap of standard 3D perovskites can be applied to their lower dimen- sional counterparts. The partial substitution of Pb^{2+} by Mn^{2+} in $CsPbBr_3$ NPs leads to a blueshift of the optical spectra, caused by a lattice contraction due to cation size variation.[44] The deep-blue emission at 456 nm was also attended with 0.2% Al doping in $CsPbBr_3$ NPs. The Al doping introduces a new energy level in the bandgap, which also contributes to the hybridization, as demonstrated in theoretical calculation.[45]

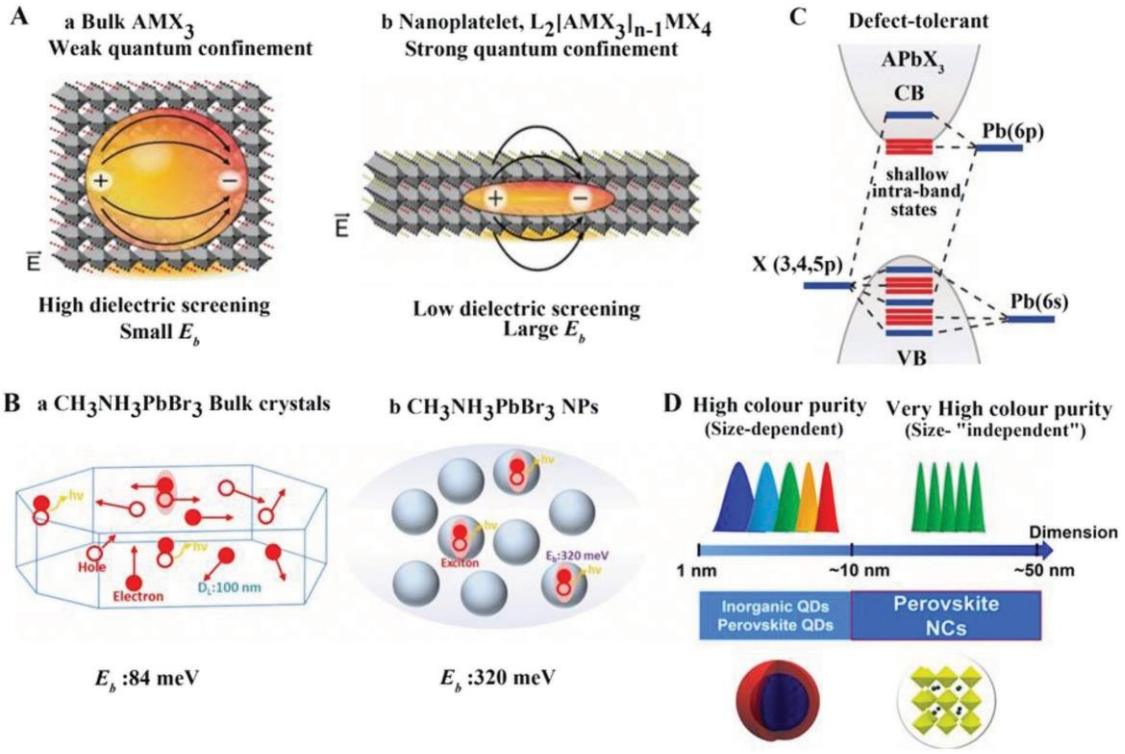

Figure 2. A) Illustration of how dielectric screening affects the electronic states differently in (A-a) cubic bulk perovskites, and (A-b) nanoplatelets. The organic medium surrounding the nanoplatelets has a much smaller dielectric constant than the perovskite layer, which is less effective in screening the electron–hole Coulomb interaction and increases the exciton binding energy (E_b) of perovskite nanoplatelets by an order of magnitude as compared to the bulk phase. Adapted with permission.[14] Copyright 2017, American Chemical Society. B) Comparison between E_b for methyl ammonium lead bromide ($CH_3NH_3PbBr_3$) bulk crystals (84 meV, few micrometers in size) and NPs (320 meV, ≈8 nm). Adapted with permission.[15] Copyright 2015, American Chemical Society. C) Defect tolerance in lead halide perovskite (LHP) NPs. Defects do not act as trap states in LHPs and are therefore benign toward their electronic and optical properties. Adapted with permission.[16] Copyright 2017, American Association for the Advancement of Science. D) Dimension distributions of inorganic QDs, perovskite QDs, and perovskite nanocrystals (NCs). Adapted with permission.[17] Copyright 2017, American Chemical Society.

2D layered perovskites of chemical formula $L_2[APbX_3]_{n-1}PbX_4$ have been particularly interesting systems to achieve the color tunability with stacking these 2D sheets in a few nanometer layer thickness. For example, nanoplate- lets of structure $L_2[FAPbX_3]_{n-1}PbX_4$ for $n = 1$ with substitution of X = I and X = Br have shown the green and violet emissions, however no emission was observed with X = Cl. Surprisingly, for $n = 2$ (thickness variation), nanoplatelets show the blue and yellow emissions for bromide and iodide substitutions, which is attributed to dielectric confinement effect (Figure 3C). In a similar fashion, by substituting Sn for Pb, the peak of emission displays a redshift. Thus, by selection of the metal (B) and halide (X), it is possible to tune the absorption/emission of the $n = 1$ and $n = 2$ nanoplatelets to span the entire visible region of the spectrum. The PL emission of the $MAPbBr_3$ nanoplatelets can easily be altered by controlling layer thickness of the plates.[46] Single-layer 2D $MAPbBr_3$ nanosheets exhibit the blueshift up to 150 meV, and can be further increased with increasing charge carrier density, ascribed to quantum and dielectric confinements as well as reduction of E_b.[46]

As previously mentioned, ion migration in halide perovskites has become a common concern in the field, with implications in current–voltage hysteresis and device degradation.[47] Initial results suggested that ion migration in polycrystalline perovskites occurs mainly through grain boundaries, which could be reduced using millimeter-sized perovskite bulk crystals.[48] However, no significant effect was observed on the hyster- esis when perovskite grain size was systematically varied.[49,50] Further, negligible device hysteresis has been also noted for vacuum deposited p–i–n and n–i–p perovskite solar cells, with average grain sizes < 50 nm.[51]

Thus, perovskite nanostructures have been proposed as possible alternatives to reduce the prejudicial effects of ionic migration, such as the phase segregation in mixed-halide perovskites. As a promising result, quasi-2D crystal structures, like Ruddlesden–Popper layered perovskites, seem to overcome the device hysteresis as well as enhance the device stability.[52]

Ion migration was reported in mixed halide $CsPbBr_{3-x}X_x$ (X = I or Cl) NP systems, with an associated redshift and splitting of the electroluminescence peaks with respect to applied voltage. Long-lived deep-red-emitting devices could be achieved using mixed halide NPs with higher compositional concentrations of iodide.[53] Approaches to confine the ions in the nanostructures could improve these effects, but further study is necessary in this direction.

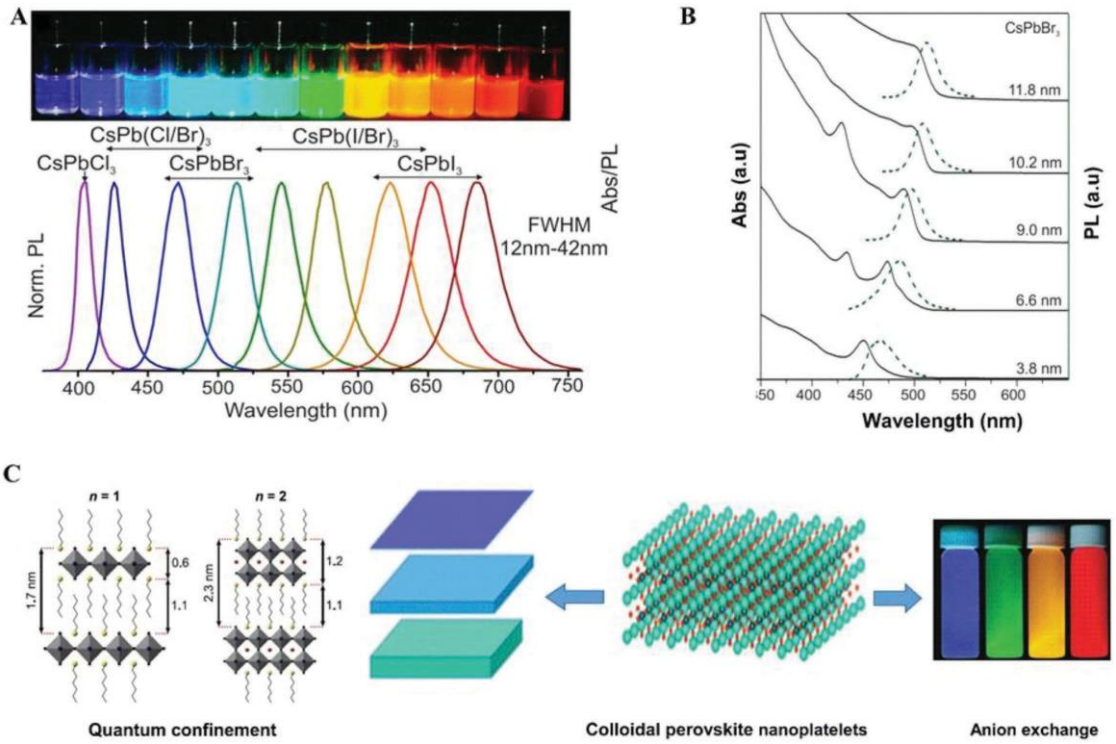

Figure 3. Representation of the color tuning of the perovskite nanocrystals and nanoplates by means of chemical tuning as well as quantum conferment effect. A) Colloidal perovskite $CsPbX_3$ NPs (X = Cl, Br, I) exhibit size- and composition-tunable bandgap energies covering the entire visible spectral region with narrow and bright emission. Colloidal solutions in toluene under UV lamp ($\lambda = 365$ nm) and the representative PL spectra ($\lambda_{exc} = 400$ nm for all but 350 nm for $CsPbCl_3$ samples). B) Quantum-size effects in the absorption and emission spectra of 5–12 nm $CsPbBr_3$ NPs. Adapted with permission.[37] Copyright 2015, American Chemical Society. C) Schematic representations of the nanoplates stacks and relevant distances for $n = 1$ and $n = 2$. Adapted with permission.[38] Copyright 2016, American Chemical Society. Color tuning with respect to quantum confinement as anion exchange approach in perovskite nanoplates. Image of colloidal perovskite nanoplatelets: Adapted with permission.[36] Copyright 2015, American Chemical Society.

3. Perovskite NP Synthesis

The ongoing developments of light emission devices based on perovskites have resulted in a growing interest in synthesis of highly luminescent perovskites NPs. They show enormous potential in various fields of optoelectronics, such as light-emitting diodes, photodetectors, transistors, lasing, etc.[11,54–58] The versatility of perovskite NPs is represented by the large amount of parameters, such as particle size, dimensionality, and chemical composition, which tune their optical and electronic properties. The manipulation in morphology and optical and electronic properties of the perovskite NPs can easily be customized by precisely controlling the experimental conditions like precursor chemical composition, concentration, reaction temperature, and time.

A number of methods have been demonstrated to synthesize the colloidal perovskite NPs namely solvent-induced reprecipitation, ligand-assisted reprecipitation (LARP), emulsion process, template assisted synthesis, and others.[59–65]

Figure 4 is a representation of perovskite NP formation by varying the different reaction conditions: A) schematic illustrating the formation process for different $CsPbX_3$ (X = Cl, Br, I) nanocrystals mediated by organic acid and amine ligands at room temperature,[66] B) influence of reaction temperature in $CsPbBr_3$ colloidal synthesis,[36] C) schematic of nanoscale solid film templates nanoporous alumina (npAAO) and nanoporous silicon (npSi) on the infused with perovskite NPs,[67] D) schematics representation of core–shell-type layer growth of octylammonium lead bromide nanomaterials over $MAPbBr_3$ NPs,[68] E) a) transmission electron microscopic (TEM) images of the nanostructures found in the octylammonium (OA)/MA perovskite suspensions along with b) photographs of the perovskite suspensions under UV light and c) PL and UV–vis spectra of perovskite films.[46]

3.1. Solvent-Induced Precipitation

In general, the kinetics of perovskite crystallization, i.e., the size of the resulting NPs, can be controlled with long chain amine ligand, whereas oleic acid suppresses aggregation and ensures the colloid stability. The initial efforts to synthesize the colloidal $MAPbBr_3$ NPs comprised the addition of perovskite precursors, lead bromide ($PbBr_2$) and methyl ammonium bromide (CH_3NH_3Br) along with oleic acid (OAc) and octylamine in a noncoordinated solvent octadecylene (ODE) into the acetone to initiate the solvent-induced precipitation at 80 °C.[65] The obtained NPs are with PLQY of 20% as well as stable in colloidal solution over three months.[59,65] Further enhancement in PLQY up to 83% could be achieved by optimizing the molar ratio of OABr:MABr:$PbBr_2$ (8:12:5), while maintaining

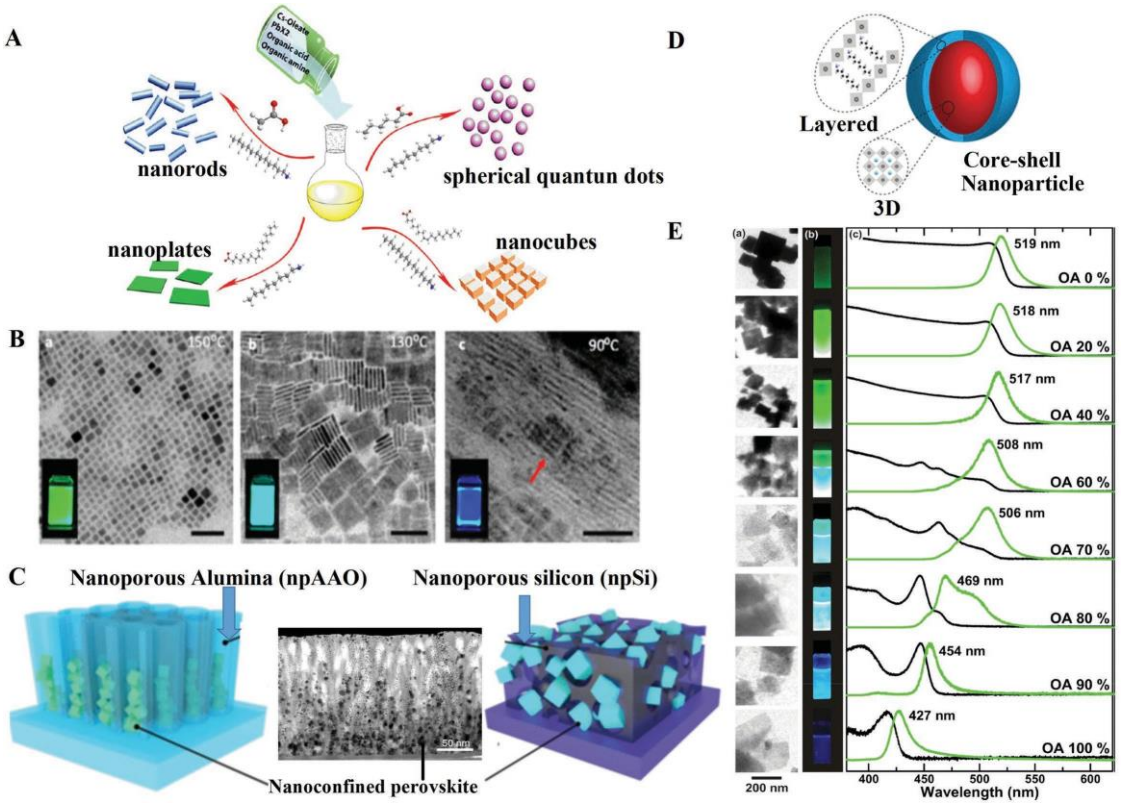

Figure 4. A) Schematic illustrating the formation process for different $CsPbX_3$ (X = Cl, Br, I) nanostructures mediated by organic acid and amine ligands at room temperature. Hexanoic acid and octylamine for spherical quantum dots; oleic acid and dodecylamine for nanocubes; acetate acid and dodecylamine for nanorods; oleic acid and octylamine for few-unit-cell-thick nanoplatelets. Adapted with permission.[66] Copyright 2016, American Chemical Society. B) Influence of reaction temperature in $CsPbBr_3$ colloidal synthesis. (B-a) At 150 °C, (green emitting 8–10 nm nanocubes). (B-b) At 130 °C, cyan emitting nanoplates with lateral dimensions of 20 nm and thickness of a few unit cells (≈3 nm) are formed. (B-c) At 90 °C, blue emitting thin nanoplates along with several hundred nanometers lamellar structures, growth along the lamellae (red arrow) (Ba–c, scale bar is 50 nm). Adapted with permission.[36] Copyright 2015, American Chemical Society. C) Schematic of nanoscale solid film templates (npAAO) and npSi infused with perovskite NPs along with the bright-field scanning transmission electron microscopy (BF-STEM) image (middle image) of a 170 nm high, ≈100 nm thick npAAO filament, indicating alumina nanopores of 6–8 nm in diameter, partially filled with conjoined perovskite nanocrystals. Adapted with permission.[67] Copyright 2017, the American Association for the Advancement of Science. D) Schematics representation of core–shell-type layer growth of octylammonium lead bromide nanomaterials over $MAPbBr_3$ NPs. Adapted with permission.[68] Copyright 2016, the Royal Society of Chemistry. E-a) TEM images of the nanostructures found in the OA/MA perovskite suspensions. E-b) Photographs of the perovskite suspensions under UV light. E-c) PL and UV–vis spectra of perovskite films prepared from the aforementioned suspensions. Adapted with permission.[46] Copyright 2015, American Chemical Society.

the 1-octadecene:$PbBr_2$ molar ratio of 62.6:1.0.[59] Similarly, synthetic approach of NP preparation was adopted by few other groups to prepare perovskite NPs of sizes below 6.5 nm for applications like photodetectors, sensors, etc.[41,69,70]

3.2. LARP

Unlike the abovementioned method, in LARP approach, perovskite precursors along with *n*-octylamine and oleic acid were dissolved into polar dimethylformamide (DMF) solvent instead of ODE, followed by a dropwise addition of fixed amount of perovskite precursor solution into toluene under vigorous stirring.[60] Using this method, the synthesis of color-tunable $CH_3NH_3PbX_3$ QDs (average diameter of 3.3 ± 0.7 nm) with absolute PLQYs in the range of 50–70% at low excitation fluence has been demonstrated.[60] As realized in temperature-dependent PL measurements, the improvement in PLQY for the $CH_3NH_3PbBr_3$ QDs (average diameter 3.3 nm, PLQY – 70%) than that of corresponding micrometer-sized bulk particles (2–8 μm, PLQY < 0.1%) is attributed to the increase of E_b (≈375 vs ≈65 meV) due to size reduction as well as proper chemical passivation of the Br-rich surface (Br:Pb ratio 3.55 vs 3.0). Further, the reduction in the average PL lifetime of QDs with respect to the bulk films (≈6 vs ≈100 ns) supports the exciton radiative recombination. Likewise, for well-defined cubic-shaped thermally stable $FAPbX_3$ nanocrystals of ≈10 nm, PLQY of 75% has been demonstrated using LARP method.[71]

A new protocol using the LARP approach has been recently demonstrated to synthesize a solution-processed, highly stable core–shell-type mixed MA–OA lead bromide perovskite NPs (≈5–12 nm) with high PLQY of up to 92%. The formation of core–shell-type NPs was accomplished by systematically altering the molar ratio of capping ligands, OABr, and MABr without changing total amount of organic ammonium bromide and synthesis conditions. The color tunability of NPs in the

blue to green spectral region (438–521 nm), high PLQY, and reasonable stability under ambient condition are credited to the quantum confinement imparted by the crystal engineering associated with core–shell NP formation.[68,72]

3.3. Emulsion Method

The emulsion method provides better control on the perovs- kite crystallization and forms a monodisperse $CH_3NH_3PbBr_3$ QDs with tunable size from 2 to 8 nm and absolute PLQYs of 80–92%.[61] This synthesis process involves the mixing of two immiscible solvents, such as DMF and *n*-hexane, to form emulsion and subsequently addition of demulsifier (for instance, *tert*-butanol/acetone), initializes solvent mixing, and induces the crystallization.[61] Moreover, it is easy to obtain the solid- state powder of NPs, which can be redissolved for thin-film coating and device fabrication. Two-step NP synthesis approach involves the initial preparation of nearly monodisperse PbI_2/ $PbBr_2$ NPs, followed by reaction with an alkyl ammonium iodide/ bromide salts to produce the respective perovskite NPs. The NPs with different layered multiple quantum well-like structures, generally denoted by $R_2(CH_3NH_3)_{n-1}PbnI_{3n+1}$; n = 1–3, correspond to perovskite layers and *R*-long chain length ligand; layered perovskites can easily synthesized by tuning ligand ratio. The obtained NPs using this approach show sharp excitonic features, and are suitable candidate to study the intrinsic photophysics and spectroscopic properties.

Although these synthesis routes of colloidal NPs can generate materials with high PLQY (≈100%),[73] the fabrication methods are very sensitive to the reaction conductions. Also, the resulting NPs often end with the mixture of different sizes and morphologies, which adversely affects its potential application.

3.4. Template-Assisted Method

In contrast to the methods discussed above, in the template-assisted approach, NP formation is induced by the crystallization kinetics on a specific substrate (as a template) rather than with the aid of organic capping ligand. For instance, the growth of monodisperse $CH_3NH_3PbBr_x$ perovskite nanocrystals takes place inside mesoporous silica[62] as well as aluminum oxide film.[74]

The resulting film exhibits an intense green emission with a narrow bandwidth and can be further optimized based on the synthesis conditions as well as type of metal oxide template. Using this approach, the perovskite NPs of different sizes as well as color tunable, green (22 nm) to near-infrared (36 nm) with PLQY of above 50%, can be easily prepared by simply infusing the perovskite precursors in using different pore size mesoporous silica or alumina templates. Recently, the strategy of confining perovskite nanocrystallites (<10 nm) directly within device relevant solid-state thin-film formats without the use of any capping ligand has also been demonstrated.[67] The method is useful for bandgap engineering through confinement in nanoporous solids as well as precisely control- ling the emission wavelength of perovskite nanoparticles in next-generation, solution-derived photonic source. Few other methods like electrospinning, pulsed-laser irradiation in liquid have also been reported for perovskite NP synthesis, which mostly result in 2D perovskite structures.[63,64]

3.5. Hot Injection Method

Perovskite NPs with all-inorganic cations have received significant attention, because of their higher thermal stability compared with the hybrid organic–inorganic perovskites. By substituting the organic MA cation with a fully inorganic one (e.g., Cs), the perovskite resistance against thermal and ambient degradation can be greatly augmented.[75,76] $CsPbX_3$ perovskites present a direct bandgap and exist in the different crystal phases depending on the temperature. For instance, $CsPbBr_3$ shows a cubic phase above 130 °C, cubic–tetragonal phase between 130 and 88 °C, and an orthorhombic one below 88 °C. During these transitions, it barely shows any color (orange) change with respect to phase formation.[77] Its narrow emission with high quantum yields (up to 90%) is the primary motivation to focus on synthesis and study their optical proper- ties for future application in optoelectronic.

The hot injection method is one of the most commonly used methods for $CsPbX_3$ NP synthesis. A typical synthesis involves the mixing of perovskite precursors, PbX_2 (X = I/Br/Cl), in ODE along with oleic acid, oleylamine, and quick injection of Cs-oleate under dry condition and at 140–200 °C.[37,42,78] The reaction can be quenched within 5–10 s either by cooling the reaction mixture in ice-water bath or with the addition of *tert*-butanol to complete precipitation. The NPs were obtained after discarding the supernatant and redispersing the precipitate either in toluene or in hexane to form stable colloidal solutions. With this approach, one can easily acquire monodisperse nanocubes, of 4–15 nm edge length and high PLQY up 50–90%, narrow emission line widths of 12–42 nm over visible spectral region of 410–700 nm, and shorter radiative lifetimes (1–29 ns). Furthermore, based on the effective mass approximation, one can calculate effective excitons Bohr radius and the binding energies for $CsPbI_3$ (6 nm, 20 meV), $CsPbBr_3$ (3.5 nm, 40 meV), and $CsPbCl_3$ (5 nm, 75 meV). Especially, the optical properties of the perovskite NPs are strongly related to their shape, size, and surface chemistry due to the change in the band structure. In fact, with the alteration of the reaction temperature, time, the surfactant ligands along with and the perovskite precursor composition[79] realized the formation of nanoplatelets,[36,78] nanowires,[77,80,81] spherical dots,[66] and nanorods.[82] In addition, small variation in the reaction temperature affects the size of the NPs, i.e., the size of the NPs decreases by decreasing the reaction temperature.[37] Notable efforts also led to the synthesis of lead-free, tin-based perovskite nanocrystal.[83] But, NP preparation using hot injection approach is very sensitive to temperature change as well as tedious to carry out as being under an inert atmosphere, consequent efforts are made to synthesize the shape-controlled $CsPbBr_3$ NPs at room temperature.[66] Few other methods, as discussed prior section, emulsion, LARP, template-assisted, and so on, are also employed for the synthesis of all-inorganic perovskite NPs. As an example, $FAPbI_3$ and $FA_{0.1}Cs_{0.9}PbI_3$ NP syntheses were demonstrated using LARP method.

3.6. Other Synthesis Methods

Recently, NP preparation has been reported using direct ultrasonication process as well as with solvent-free mechanosyn- thesis strategy. These are the simple, scalable, single-step, and polar-solvent-free synthesis approach to prepare a high-quality colloidal $CsPbX_3$ (X = Cl, Br, and I) perovskite NC with tun- able halide ion composition and thickness of the corresponding precursor solutions in the presence of organic capping mole-cules.[84] Their composition can be adjusted conveniently simply through mechanically milling/grinding stoichiometric combinations.[85]

A method of partial cation exchange in $CsPb_{1-x}MxBr_3$ NPs of Pb^{2+} with isovalent cations ($M = Sn^{2+}$, Cd^{2+}, and Zn^{2+}; $0 < x \leq 0.1$) have been demonstrated. The isovalent cation doping perverses the original size and shape of the NPs with a bit contraction of the unit cells, which leads to a blueshift of the optical spectra, while maintaining the high photolumi-nescence quantum yields (>50%), with narrow emission of the parent $CsPbBr_3$ NPs. The blueshift in the optical spectra is attributed to the lattice contraction that accompanies the Pb^{2+} for M^{2+} cation exchange and observed to scale linearly with the lattice contraction. This work opens up new possi- bilities to engineer the properties of halide perovskite NPs, which to date are demonstrated to be the only known system where cation and anion exchange reactions can be sequen- tially combined while preserving the original NP shape, resulting in compositionally diverse perovskite NPs.[44] **Table 1** summarizes a few selected representative perovskite LEDs (PeLEDs) fabricated using the perovskite NPs synthe-sized by different synthesis methods. The highest reported external quantum efficiency (EQE) of 13.4% for the $FAPbBr_3$ NPs (≈10–15 nm) was synthesized using simple LARP method.

3.7. Synthesis of Other Lower Dimensional Nanostructures

A metal halide perovskite in the form of nanosheets/nano-platelets (2D) or nanowires (1D) have also acquired a great importance in building blocks for future perovskite-based nanoscale optoelectronic and photonic devices.[14] They exhibit the high excitonic binding energy, strong dielectric and quantum confinement, as well as enhanced radiative recombi- nation as compared to the bulk counterpart. In addition, their large surface area enables their stronger interaction with the 2D materials for efficient energy or electron transfer. Ini- tially, the formation of the colloidal perovskite nanoplatelets was observed as an addition product during the synthesis of $MAPbBr_3$ NPs and which was identified due to the blueshift in the absorption and emission spectra mainly because of strong quantum confinement effect.[70] The 3D perovskite NPs can be easily tailored into 2D nanosheets or 1D nanowire structure by varying the amount of long chain cation in the precursor solu-tion during the course of synthesis.[86] The direct growth of nanosheets or nanowires on a substrate surface has also been demonstrated, and it is plausible to produce nanoplatelets with lateral dimensions in the 1–10 μm range also, with careful control of the solvent composition possible to growth of atomi-cally thin single-layer nanoplatelets. The direct conversion of $CH_3NH_3PbI_{3-x}Cl_x$ perovskite thin films into nanowires has also been illustrated through dissolution-recrystallization process. The nanowires are of 0.1–1 μm in diameter and exhibit excel-lent optical properties for flexible photodetector application.[87] In addition, high crystalline quality freestanding $CH_3NH_3PbI_3$, $CH_3NH_3PbBr_3$, and $CH_3NH_3PbI_xCl_{3-x}$ perovskite nanowires have also been shown with vapor phase method.[88] The optical-pumped room-temperature $CH_3NH_3PbI_3$ nanowire lasers with near-infrared wavelength of 777 nm, low threshold of 11 μJ cm^{-2}, and a quality factor as high as 405. Furthermore,

Table 1. Summary of selected representative PeLEDs based on the perovskite NPs synthesized using different synthesis methods.

Number	Perovskite	Synthesis method	PLQY [%]	Device structure	Luminance [cd m^{-2}]	Current efficiency [cd A^{-1}]	EQE [%]	Ref.
1	$MAPbBr_3$ (2–8 nm)	Emulsion	80–92	Indium tin oxide (ITO)/PEDOT/Per/TPBI/CsF/Al	410	4.5	1.1	[61]
2	$MAPbBr_3$ (60 nm)	LARP	≈90	ITO/PEDOT:PSS/poly(9-vinylcarbazole) (PVK)/Per/TPBI/LiF/Al	2398	3.72	1.06	[92]
3	$FAPbBr_3$ (10–15 nm)	LARP	55–65	ITO/PEDOT:PSS/Per/B_3PYMPM or TPBI/Cs_2CO_3/Al	2714	6.4	–	[93]
4	$CsPbBr_3$ (8 nm)	Hot injection	>85	ITO/PEDOT:PSS/PVK/Per/TPBI/LiF/Al	946	0.43	0.12	[94]
5	Amorphous $MAPbBr_3$ (6.1 nm)	Nontemplate/solvent-induced precipitation	≈77	ITO/PEDOT:PSS/poly-TPD/Per/TPBI/4,6-Bis(3,5-di(pyridin-3-yl)phenyl)-2-methyl-pyrimidine (B_3PYMPM)/Cs_2CO_3/Al	1189	11.49	3.8%	[95]
6	$CsPbBr_3$ (40 nm)	Hot injection	–	ITO/PEDOT:PSS/poly(4-butylphenyl-diphenyl-amine)(poly-TPD)/perfluorinated ionomer (PFI)/Per/TPBI/LiF/Al	1377	0.19	0.06	[96]
7	$CsPbBr_3$	Hot injection	50–60	ITO/ZnO/Per/TPBI/MoO_3/Ag	2335	–	0.19	[97]
8	$CsPbBr_3$ (20 nm)	Hot injection		ITO/PEDOT:PSS/poly-TPD/Per/TPBI/LiF/Al	15 185	13.3	6.27	[98]
9	$FAPbBr_3$ (10–15 nm)	LARP	≈80	ITO/PEDOT:PSS/Per/2,4,6-tris[3-(diphenylphosphinyl)phenyl]-1,3,5-triazine (POT2T)/Ca/Al	34 480	57.6	13.4	[99]

the graphoepitaxial nanowire array growth in open nanofluidic channels has open up possibility of fabrication of controlling size, shape and oriented wafer-scale perovskite nanowire thin films for application in various optoelectronic devices.[89,90] The 2D nanoplatelets can also be prepared from the bulk material into a mixture of nanocrystals and nanoplatelets stabilized by the coordinating solvents through liquid exploitation method.[91]

4. From 3D Perovskite to Perovskite Nanoparticle PeLEDs

In earlier attempts to fabricate light-emitting devices based on perovskite-related compounds, more than two decades ago, electroluminescence could only be achieved at liquid nitrogen temperatures[100] and at very high applied voltage,[101] thus limiting their practical application. More recently, following the rise of perovskite solar cells, the PeLEDs fabricated with $CH_3NH_3PbI_{3-x}Cl_x$ films (15 nm) demonstrated an infrared radiance of 13.2 W sr^{-1} m^{-2} at a current density of 363 mA cm^{-2}, with highest external and internal quantum efficiencies of 0.76% and 3.4%, respectively.[11] However, the pinholes or poor coverage of the perovskite films limit the device quantum effi- ciency through nonradiative current losses, and can even lead to early breakdown at lower bias voltages due to local joule heating effect.[102] A triple-cation perovskite formed with incorporation of Cs cation into $MA_{0.17}FA_{0.83}Pb(Br_xI_{1-x})_3$ [103] formulation, along with the suitable electron transport layer (ETL) and hole transport layer (HTL) for balanced change transfer, obtained the red, green, and blue PeLEDs with unprecedentedly EQEs of 9.23%, 7.3%, and 1.7%, respectively.[104] Furthermore, $CsPbX_3$ (X = Cl, Br, I)-based pure inorganic system reveals excellent thermal stability and high PLQY. The excess of CsBr or polymer addition in $CsPbBr_3$ precursors significantly reduces the trap density and thus leads improved PeLED performance. [105,106]

High electroluminescence efficiency could be accomplish circumventing nonradiative paths, such as Auger processes and trap-mediated recombination. In typical PeLED working conditions, charge-carrier density is lower than 10^{15} cm^{-3}, only slightly higher or even comparable to the trap densities obtained for 3D perovskites by some reports.[107–109] Therefore, the EQE in 3D films is greatly hampered by effective competition between the defect-states trapping (first order decay process) with the slow electron–hole bimolecular radiative recombination (second order decay process). Additionally, the usually low E_b in the bulk perovskites could hinder further improvements in their charge to photon conversion efficiency.[110,111] Under thermodynamic equilibrium conditions, depending on the E_b and excitation density, free charge and exciton coexistence and interaction may affect the radiative recombination. In order to counterbalance these effects, the field has aimed the charge confinement. Therefore, high-efficiency PeLEDs have been accomplished by controlling the size of the perovskite nanoparticles, reducing the thickness of active regions and using the reduced-dimensionality perovskite emitters to spatially confine the carriers and thus enhance radiative recombination.[11] Unfortunately, this can spatially limit the diffusion length of excitons or charge carriers.

In line with the trend in the field, toward a progressive reduction of the thin-film grains, a novel approach of nanocrystal pining (NCP) in 3D films was demonstrated, where a small organic molecule, 2,2′,2″-(1,3,5-benzinetriyl)-tris(1-phenyl-1-*H*-benzimidazole) (TPBI) was added in the chloroform during the film formation process. The $MAPbBr_3$ film formed with this process showed the reduction of grain size in the range of 50–150 nm. Two factors drove the improvement of the devices by and addition of excess MABr: the minimized grain boundaries and smaller diffusion length ($L_D \approx 67$ nm).[112] The reduction of L_D was attributed to the reduced grain size, in which excitons are under stronger spatial confinement,[11] thereby reducing dissociation and enhancing radiative recombination. The devices fabricated with this process showed a maximum current efficiency (CE) of 42.9 cd A^{-1} with an EQE of 8.53%, comparable to that of organic LEDs.[11] The addition of long chain ammonium halides (such *n*-butylammonium halides) in the precursor solution impedes the growth of 3D perovskite grains, decreases the film roughness (≈1 nm), as well as features a transition from 3D to Ruddlesden–Popper structures.[113,114] For instance, 4-fluorophenylmethylammonium iodide/bromide addition leads to NP thin film of mean crystal sizes of 5.4 ± 0.8 and 6.4 ± 1.3 nm and results into PeLED EQE values of 7.9% and 7% for $MAPbI_3$ and $MAPbBr_3$, respectively.[115] A highly luminescent $MAPbBr_3$ nanocrystalline in situ thin-film formation[116] was also accomplished with combination of Lewis acid–base adduct[117] as well as nonthermal solvent–vacuum film drying method. The excess of MABr in the precursor solution controls the crystal growth of $MAPbBr_3$ and remains at periphery of $MAPbBr_3$ nanoparticles, thus forming a type I band alignment.[116] Similarly, devices based on amorphous $CH_3NH_3PbBr_3$ NPs (**Figure 5**A,B) displayed external quantum yield close to 4%.[95]

Following the reduction of the grain size in PeLEDs, perovskite NPs attracted the attention of the light emission field as a natural step. Partially replacing methyl ammonium bromide by octyl ammonium bromide resulted in the in situ formed nanocrystals, displayed signatures associated with excitonic recombination, rather than that of bimolecular recombination of 3D perovskites, which indicates a clear transition toward NP films. This was accompanied by enhanced photoluminescence PLQY of 20.5% in comparison with that of 3.40%.[118]

When synthesized using the colloidal approach, they can exhibit large E_b, low charge carrier diffusion length (L_D), and high PLQY at room temperature. PeLEDs based on colloidal NPs have also been demonstrated employing the organic–inor- ganic as well as inorganic perovskite NPs .[119] The strategies like uniform film formation as well as suitable device con- figuration for balance charge injection into emitter has been employed to achieve better performance.[96,120] Devices fabri- cated with a $CH_3NH_3PbBr_3$ QDs (2–8 nm) prepared using the emulsion method exhibited maximum current efficiency of 4.5 cd A^{-1}, and EQE of 1.1%.[61]

In another approach, a new trimethylaluminum (TMA) vapor–based crosslinking method was used to render the $CsPbI_3$ nanocrystal films and yield higher EQE of 5.7% than the non-crosslinked device. Usually, the aliphatic ligands on the nanocrystals are easily soluble in organic solvents, which limit subsequent deposition of ETL using solution methods, TMA crosslinking method overcomes this problem by effectively creating aluminum oxide network between the NPs.

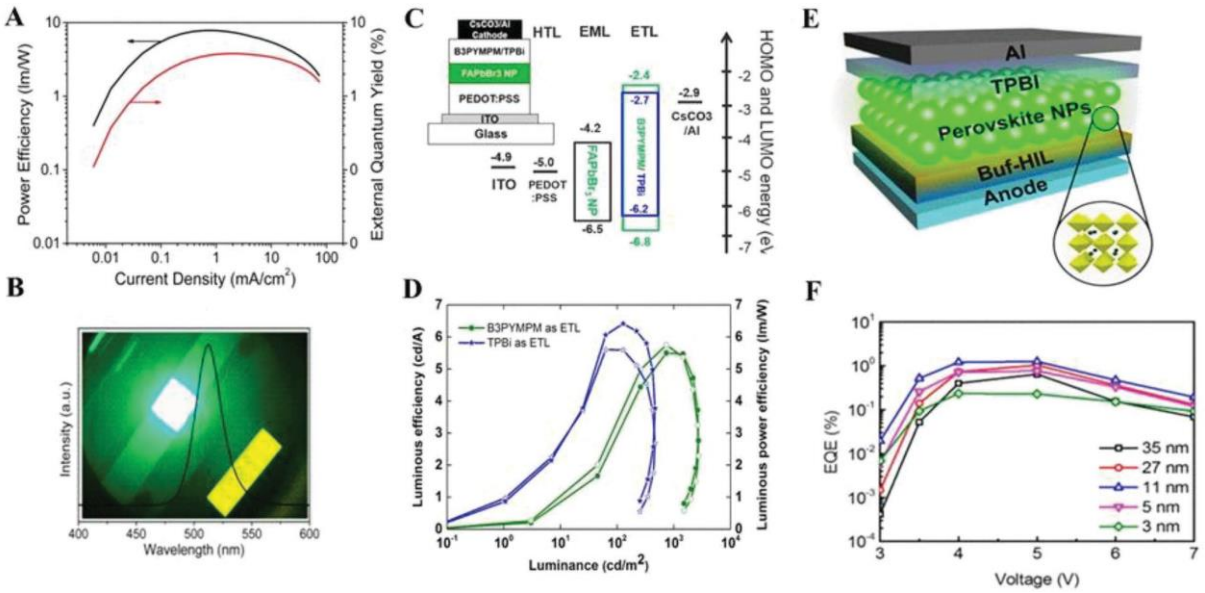

Figure 5. A) PeLED based on the amorphous $CH_3NH_3PbBr_3$ NPs. Illustration of power efficiency–current density (black) and external quantum yield–current density (red), and B) the image of the resulting device operating at a luminance of 1189 cd m^{-2} and characteristic electroluminescence spectra at a peak wavelength of 512 nm, and with a FWHM of 26 nm. Adapted with permission.[95] Copyright 2016, Elsevier Ltd. C) PeLED based on the $FAPbBr_3$ NPs (10–15 nm). Schematic energy level diagram for the materials used for device fabrication and D) characteristics luminous efficiency (cd A^{-1}) versus luminance (cd m^{-2}) and luminous power efficiency (lm W^{-1}) versus luminance (cd m^{-2}). Adapted with permission.[93] Copyright 2016, Nature Publishing Group. E) PeLED based on various sizes of NPs device structure and F) characteristic EQE. Adapted with permission.[17] Copyright 2017, American Chemical Society.

Furthermore, this method was also demonstrated to various RGB-emitting PeNP films. A simple dip-coating method has been reported to fabricate large-area uniform films for PeLEDs using perovskite NPs and shown the blue, green, and red, current efficiency of 4.01, 3.72, and 1.52 cd A□ 1, and an EQE of 1.38%, 1.06%, and 0.53%, respectively, with long-term stability in air (humidity ≅ 50%) for at least 7 days.[92]

Similarly, devices fabricated using colloidal $FAPbBr_3$ NPs, PLQY of 55–65% demonstrate luminous efficiency of 6.4 cd A^{-1} and peak luminous power efficiency of 5.7 lm W^{-1} (Figure 5C,D).[93] The all-inorganic perovskite $CsPbX_3$ QD–based blue, green, and yellow LEDs with sharp emissions (full-width at half maximum (FWHM) □ 30 nm) exhibited a luminance of 742, 946, and 528 cd m^{-2}, with EQE of 0.07%, 0.12%, and 0.09%, respectively.[94] The efficient blue LEDs based on the colloidal have been demonstrated using quantum confined 2D perovskites, with precisely controlled stacking down to one-unit-cell thickness (n = 1).[121] The high-performance PeLEDs based on the colloidal MAPbBr3 (6 nm) amorphous NPs have been dem- onstrated, current efficiency of 11.49 cd A^{-1}, and EQE of 3.8%.[95] Recently, the colloidal perovskite NCs in a dimension greater than Bohr diameter have been demonstrated a high PLQY (≅60.5%) in a compact film for reported the a high CE of 15.5 cd A^{-1} highly efficient light-emitting diodes by using a multifunctional buffer hole injection layer (Buf-HIL). The Buf-HIL composed of poly(3, ethylenedioxythiophene)/polystyrene sulfonate (PEDOT:PSS) and perfluorinated ionomer induces uniform perovskite particle films with complete film coverage and prevents exciton quenching at the PEDOT:PSS/perovskite particle film interface (Figure 5E,F).[17]

5. Nanoparticles for Photovoltaics: Beyond the Shockley–Queisser Limit

PLQY of the perovskite NPs and quasi-2D is a measure of brightness, considered as one of the most important aspects for high performance light-emitting materials. However, it is also a key indicator of the general optoelectrical material property. The recombination path of the photoexcited species, which is influenced by a number of factors such as excitation or charge carrier density and temperature determine the PLQY. In the 3D halide perovskites, charge carrier recombination takes place through monomolecular recombination, bimolecular recombination, or Auger recombination processes and can be described by the simple Equation (1) as given below[122,123]

$$\frac{dn(t)}{dt} = G - k_1 n - k_2 n^2 - k_3 n^3 \quad (1)$$

where n stands for the carrier density, G is the generation rate, k_1 represents the monomolecular recombination constant (typically trap mediated), k_2 is free carrier bimolecular recombination coefficient, and k_3 is the Auger recombination coefficient. A "monomolecular" charge-carrier recombination process involves a single charge carrier, i.e., electron, hole, or an exciton (bound electron–hole pair), which mainly recombines with the defects or traps presents in the bandgap region. It is also called

Shockley–Read–Hall (SRH) recombination. This defects or traps states can occur during the material processing because of low crystallinity or material impurities. It decreases monotonically with decreasing temperature and can be overcome by controlling the trap/defect states through surface passi- vation. The bimolecular radiative type of recombination occurs when an electron from the conduction band directly combines with a hole in the valence band and releases a photon of sim- ilar energy. This is an intrinsic radiative recombination pro- cess usually invariant with defects states. Thus, increasing the weight of bimolecular recombination rate offers a high PLQY. Auger recombination of charge-carriers is a many-body nonra- diative process comprises a recombination of an electron with a hole, accompanied by recombination energy and momentum is transferred to an additional carrier either electron or hole, recognized as Auger electron or hole[122] and is most signifi- cant at high carrier concentrations. In many colloidal QDs, the Auger recombination time takes place in the picosecond range and efficiently quenches the light emission.[124]

Usually, PLQY is controlled by k_1 and charge carrier density (n) at the typical working conditions of the PeLED. It is limited at low charge carrier density because of the charge trapping at defects sites, while at high carrier density, the traps states are mostly filled and recombination of the photogenerated spe- cies is dominated by radiative processes.[125] Similarly, at low temperature, there are less number of traps states and most of them are filled at given carrier density hence the high PLQY could be noted at low temperature. Surprisingly, it could possible to reach ≈95% of PLQY at 190 K.[108]

The PLQY boost with reduction in size discussed here is mainly due to quantum confinement effect, which promotes efficient radiative recombination.[60] NPs show high surface area to volume ratio, nevertheless the high PLQY with respect to 3D films seems to indicate that surface states are not gen- erating nonradiative pathways, or these are passivated by the capping ligands. Actually, high PLQY can be achieved with the different nanostructures like nanowires, nanoplatelets, and nanorods.[36,37,120,126] Similarly, 2D perovskite nanoplatelets exhibit the confinement effect in only one direction, leading to large exciton binding energies and high PLQY. These inter- esting emission properties of perovskite nanostructures are a sign of the suppression of nonradiative recombination path- ways. The strategy of improving emission characteristics to enhance the photovoltaic performance represented a break- through in GaAs photovoltaics, which resulted in the most efficient solar cells to date.[127] Thus, the development of high PLQY NPs and quasi-2D perovskites represents an opportunity not only for light emission applications, but also for photovol- taics.[128] The photon-recycling strategy enabled by the high PLQY has already been proven in 3D films.[129] This consists in a better management of the absorbed photons, which can be re-emitted and reabsorbed several times, reducing the losses.

As a first step, solar cells based on $CsPbI_3$ NPs have achieved one of the highest open circuit potentials (1.23 V) of the perovskite field with the standard TiO_2 and 2,2′,7,7′-tetrakis(*N*,*N*-di-*p*-methoxyphenyl-amine)9,9′-spirobifluorene (spiro-OMeTAD) as electron and hole transporting layers, respectively, as represented in **Figure 6**.[128] These NPs retained cubic structure, and their size (from ≈3 to ≈15 nm) determined the absorption onset of the solar cell (from ≈585 to ≈670 nm wavelength). Improving the mobility in these systems by cation-halide

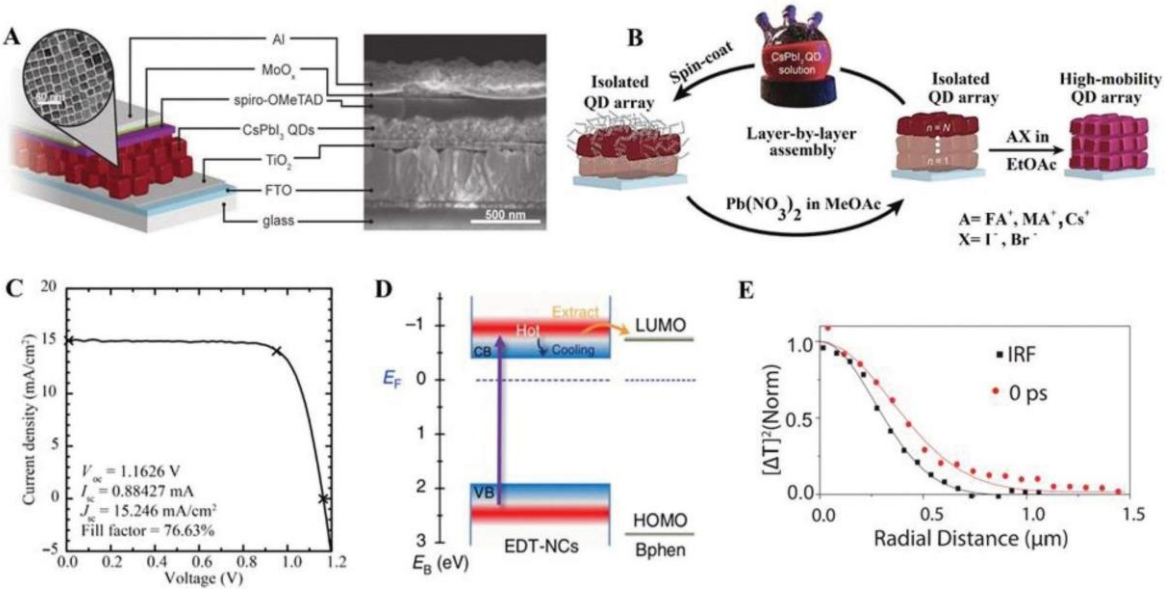

Figure 6. A) Schematic representation and cross-section scanning electron microscopic (SEM) image of a perovskite. Adapted with permission.[128] Copyright 2016, American Association for the Advancement of Science. B) Fabrication procedure and C) performance of a $CsPbI_3$ NP solar cell. Adapted with permission.[130] Copyright 2017, American Association for the Advancement of Science. D) Schematic representation of the hot-carrier extraction mechanism. Adapted with permission.[131] Copyright 2017, Nature Publishing Group. E) Hot-carrier distribution at 0 ps delay for 3.14 eV excitation over a radial distance obtained by averaging all angles compared to the instantaneous rotating frequency (IRF), as defined in the text. Adapted with permission.[132] Copyright 2017, American Association for the Advancement of Science.

treatments resulted on certified efficiencies of 13.43%, the record for quantum-dots solar cells to date.[130] Similarly, several reports on lower dimensionality perovskite solar cells denote the field's potential.[21,133–138] As it happens with light- emitting devices based on these nanostructures, the main performance improvement route is the charge transport enhancement. Beyond conventional photovoltaics, halide perov- skite nanostructures have opened new hopes in overcoming the SQL for single junction devices. This detailed balance or SQ limit refers to the maximum theoretical solar conversion efficiency limit of 33.7% that can be achieved with a single absorber layer with a bandgap of ≈1.3 eV (under the AM
1.5 solar spectrum).[139] Efficiency is mainly limited by intrinsic factors such as bandgap of the absorber, geometric factor, and various nonradiative recombination losses. More specifically, the solar cell cannot absorb photons with energy less than the bandgap while high energy photons are still capable of only exciting one carrier. These high-energy carriers with the excess of kinetic energy (kT) larger than the semiconductor bandgap are commonly designated as "hot carriers." Usually, during the process of hot carrier relaxation, the excess of energy is transferred to lattice though carrier-phonon interactions generally termed as "thermalization." Thermal equilibration of these carriers with bulk solid are known as a carrier "cooling," the phonons involved in this process are the longitudinal optical (LO) phonons. Thermalization or carrier relaxation processes which (occur rapidly within <100 fs[140]) in the bulk film is a major loss process underpinning the SQ limit for power conversion efficiencies.[141] These processes, which have been widely studied in general photovoltaic theory, are generalized in **Figure 7**. The loss pathway can be overcome by generating hypothetical device architectures to extract the hot carriers with an energy selective contact (ESC) before they thermalize.[141,142] The main challenge is to harvest the hot carriers within a short distance before they travel and lose excess energy to the lattice in a picosecond time scale. This could be only possible by utilizing the unique properties of nanoparticles in prototype solar cells. NPs have a great potential to provide unique pathways for charge carriers; because of the presence of discrete energy levels (phonon bottleneck, i.e., a diminished subpopulation of phonon states), carrier phonon coupling is reduced, which

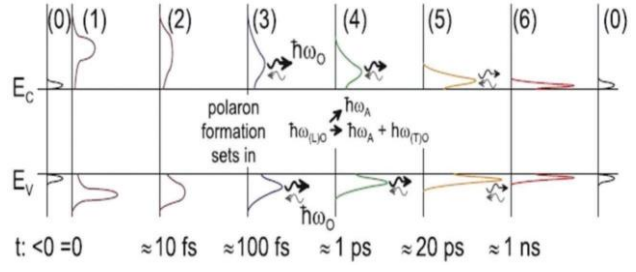

Figure 7. Timescales of general thermalization processes in semiconductors from thermal equilibrium (0). Immediately after optical generation (1) carrier–carrier scattering redistributes the energy of the carriers, forming a hot-carrier distribution (2). Optical phonon ($\hbar\omega_O$) emission and reabsorption (3); decay of optical into acoustic phonons ($\hbar\omega_A$) (4); further phonon emission (5), to thermal equilibrium; and onset of carrier recombination (6). E_C and E_V represent conduction and valence bands, respectively. Adapted with permission.[142] Copyright 2010, Elsevier Ltd.

controls the energy flow though quantum confinement effects. This has been previously demonstrated for GaAs quantum dots.[143,144] The interplay between photogenerated charge car- riers and phonons in methyl ammonium lead iodide perovskite films leads to slow thermalization of hot carriers, an indica- tion of a phonon bottleneck formation.[145–147] Following these studies, slow thermalization lifetimes have been also observed in $CH_3NH_3PbBr_3$ single crystals and $CsPbI_3$,[148] as theoreti- cally predicted.[149]

Recent results showed how the slow hot-carrier thermalization in this family of materials coexists with long diffusion lengths,[132] which for the first time enables the possibility to efficiently extract the additional energy before it is lost by thermalization. More interestingly, the use of nanostructures becomes a key tool to tune the hot-carrier dynamics in the perovskite families. Typically, the restructuring of the energy levels due to the confinement has been a recurrent approach to achieve slower thermalization.[140,142,150] Therefore, the promising phonon bottleneck measurements in the bulk perovskites could be boosted by the use of NPs, as measured in $FAPbI_3$ NPs.[151] Experimental work has already demonstrated the extraction of hot carriers[131] in $CH_3NH_3PbBr_3$ NPs under high pump fluence, with an estimated hot-carrier diffusion length of 16–90 nm. Further thermalization lifetime increases could be key to achieve different approaches to surpass the SQL, such as the realization of hot-carrier or multiple exciton generation solar cells.

6. Future Prospects

The high efficiency of thin-film metal halide perovskites in solid-state devices few years ago was an unexpected surprise for the photovoltaic community, and the exotic properties displayed by the nanoparticles open up further avenues especially in light-emitting diodes and lasing. Perovskites have demonstrated excellent coherent light emission properties and exhibited the transition from spontaneous emission (SE) to amplified spontaneous emission (ASE) with increasing pump fluence. The initial study revealed the intrinsic gain properties of $CH_3NH_3PbI_3$ film (≈65 nm) in a cavity-free configuration and reported an ASE threshold fluence of 10 ± 2 μJ cm^{-2} .[57] The essential parameters required for ideal lasing material to achieve a better ASE are low bulk defect densities (such as vacancies, interstitials), reduced nonradiative recombination, longer carrier lifetimes (approximately nanoseconds), long diffusion lengths (μm), wavelength tunability, high PLQY as well as the capability of attaining population inversion .[3,4,125] Therefore, the perovskite nanostructures and low dimensional systems have attracted attention as gain media in order to overcome the limitations of the bulk films and to achieve a better performance.[42,152] Perov- skite nanowire (NW) lasers are promising building blocks for fully integrated nanoscale photonic and optoelectronic devices, where each NW can act as a waveguide along the axial direc- tion and the two end facets form a Fabry–Perot cavity for optical amplification.[153–156] All-inorganic perovskite–based $CsPbX_3$ halide NWs are considerably more robust than the organic–inorganic counterparts and was reported to have an onset of 5 μJ cm^{-2} with a quality factor of 1009 ± 5. Further demonstrations include the high device stability under near-ambient conditions

as well as under continuous pulsed excitation for over 1 h (equivalent to 10^9 excitation cycles).[151,157]

During the preparation of the paper, reports on high performance PeLEDs have been published based on perovskite NPs. PeLEDs fabricated using $FAPbBr_3$ NPs of graded size coupled with microplatelets of octylammonium lead bromide perovskites, utilizing the energy cascade approach, has resulted in an impressive current efficiency of 57.6 cd A^{-1} and an EQE of 13.4%.[99] PeLEDs based on NPs therefore show the poten- tial for further performance improvement with material and device engineering. The recent advances in perovskite NPs allow planning a new generation of light harvesting and emission devices, including device concepts beyond conventional optoelectronics. In order to fulfill the requirements of these objectives, nanostructure-based devices will have to make full use of their high PLQY (indicative of reduced losses), while enhancing their charge transport properties to the level of their 3D films counterparts. Quantum confinement effects have been classically proposed to create optoelectronic approaches beyond the SQL, which would the basis of photovoltaic devices, and reciprocally LEDs surpassing the efficiency of the current technologies. These can include, for instance, multiple exciton generation or hot-carrier solar cells. Thus, NPs are particularly suitable systems for this purpose, and promising thermalization lifetimes have been demonstrated. Further enhancement of the hot-carrier lifetimes through quantum tuning and phonon management, long hot-carrier diffusion lengths, and suitable contacts would be crucial to achieve that long-pursued objective.

In addition to these fundamental approaches, a few practical considerations also need to be addressed. A number of methods have been reported for NP synthesis and small variation in the reaction condition (like temperature, precursor concentration, and composition) can affect their properties drastically. This, in addition to "lab-to-lab" variation in the preparation and device fabrication conditions can affect the performance of NP-based devices. In order to overcome this, there is a need to define standard protocols and exhaustive reporting of the synthesis as well as device fabrication conditions to attain reproducibility. In addition, although perovskite NPs currently show better PLQY over the bulk 3D films, the formation of functional films from colloidal NPs while keeping their physical and chemical integrity remains as a major challenge. Common limitations are ligand dissociation during isolation and purification of NPs which leads to aggregation, solvent attack during the deposition of subsequent device layers, and resistive losses due to long chain organic capping/stabilizing ligands such as oleic acid and oleylamine. PLQY is significantly reduced upon thin-film formation mainly due to NPs aggregation and a reduction of the charge confinement. Furthermore, the stability (environmental as well as thermal) of the perovskite NPs is one of the most important issues that needs further attention.

All in all, perovskite nanoparticles assure future exciting developments in the electronic fields, and are in a perfect position to attempt classically elusive objectives.

Acknowledgements

This research was supported by the National Research Foundation, Prime Minister's Office, Singapore under its Competitive Research Programme (CRP Award No. NRF-CRP14-2014-03) and through the Singapore–Berkeley Research Initiative for Sustainable Energy (SinBeRISE) CREATE Program. P.P.B. thanks the Generalitat Valenciana for funding under the project SEJI/2017/12 and the Spanish Ministry of Economy and Competitiveness (MINECO) for his postdoctoral RyC contract and the MAT2017-88905-P project.

Conflict of Interest

The authors declare no conflict of interest.

Keywords

dimensionality, light emission, nanoparticles, perovskites, photovoltaics

[1] A. Kojima, K. Teshima, Y. Shirai, T. Miyasaka, *J. Am. Chem. Soc.* **2009**, *131*, 6050.
[2] S. De Wolf, J. Holovsky, S.-J. Moon, P. Löper, B. Niesen, M. Ledinsky, F.-J. Haug, J.-H. Yum, C. Ballif, *J. Phys. Chem. Lett.* **2014**, *5*, 1035.
[3] G. Xing, N. Mathews, S. Sun, S. S. Lim, Y. M. Lam, M. Grätzel, S. Mhaisalkar, T. C. Sum, *Science* **2013**, *342*, 344.
[4] S. D. Stranks, G. E. Eperon, G. Grancini, C. Menelaou, M. J. P. Alcocer, T. Leijtens, L. M. Herz, A. Petrozza, H. J. Snaith, *Science* **2013**, *342*, 341.
[5] W. S. Yang, J. H. Noh, N. J. Jeon, Y. C. Kim, S. Ryu, J. Seo, S. I. Seok, *Science* **2015**, *348*, 1234.
[6] H. Zhou, Q. Chen, G. Li, S. Luo, T.-B. Song, H.-S. Duan, Z. Hong, J. You, Y. Liu, Y. Yang, *Science* **2014**, *345*, 542.
[7] M. Liu, M. B. Johnston, H. J. Snaith, *Nature* **2013**, *501*, 395.
[8] J. Burschka, N. Pellet, S.-J. Moon, R. Humphry-Baker, P. Gao, M. K. Nazeeruddin, M. Gratzel, *Nature* **2013**, *499*, 316.
[9] M. M. Lee, J. Teuscher, T. Miyasaka, T. N. Murakami, H. J. Snaith, *Science* **2012**, *338*, 643.
[10] H. Cho, S.-H. Jeong, M.-H. Park, Y.-H. Kim, C. Wolf, C.-L. Lee, J. H. Heo, A. Sadhanala, N. Myoung, S. Yoo, S. H. Im, R. H. Friend, T.-W. Lee, *Science* **2015**, *350*, 1222.
[11] Z.-K. Tan, R. S. Moghaddam, M. L. Lai, P. Docampo, R. Higler, F. Deschler, M. Price, A. Sadhanala, L. M. Pazos, D. Credgington, F. Hanusch, T. Bein, H. J. Snaith, R. H. Friend, *Nat. Nanotechnol.* **2014**, *9*, 687.
[12] Y. Zhao, X. Xu, X. You, *Sci. Rep.* **2016**, *6*, 35931.
[13] Z. Long, H. Ren, J. Sun, J. Ouyang, N. Na, *Chem. Commun.* **2017**, *53*, 9914.
[14] M. C. Weidman, A. J. Goodman, W. A. Tisdale, *Chem. Mater.* **2017**, *29*, 5019.
[15] K. Zheng, Q. Zhu, M. Abdellah, M. E. Messing, W. Zhang, A. Generalov, Y. Niu, L. Ribaud, S. E. Canton, T. Pullerits, *J. Phys. Chem. Lett.* **2015**, *6*, 2969.
[16] M. V. Kovalenko, L. Protesescu, M. I. Bodnarchuk, *Science* **2017**, *358*, 745.
[17] Y.-H. Kim, C. Wolf, Y.-T. Kim, H. Cho, W. Kwon, S. Do, A. Sadhanala, C. G. Park, S.-W. Rhee, S. H. Im, R. H. Friend, T.-W. Lee, *ACS Nano* **2017**, *11*, 6586.
[18] S. A. Veldhuis, P. P. Boix, N. Yantara, M. Li, T. C. Sum, N. Mathews, S. G. Mhaisalkar, *Adv. Mater.* **2016**, *28*, 6804.

[19] B. Saparov, D. B. Mitzi, *Chem. Rev.* **2016**, *116*, 4558.
[20] V. D'Innocenzo, G. Grancini, M. J. P. Alcocer, A. R. S. Kandada, S. D. Stranks, M. M. Lee, G. Lanzani, H. J. Snaith, A. Petrozza, *Nature Commun.* **2014**, *5*, 3586.
[21] T. M. Koh, V. Shanmugam, J. Schlipf, L. Oesinghaus, P. Müller-Buschbaum, N. Ramakrishnan, V. Swamy, N. Mathews, P. P. Boix, S. G. Mhaisalkar, *Adv. Mater.* **2016**, *28*, 3653.
[22] U. Rau, *Phys. Rev. B* **2007**, *76*, 085303.
[23] C. C. Stoumpos, C. D. Malliakas, M. G. Kanatzidis, *Inorg. Chem.* **2013**, *52*, 9019.
[24] N. Kitazawa, Y. Watanabe, Y. Nakamura, *J. Mater. Sci.* **2002**, *37*, 3585.
[25] J. H. Noh, S. H. Im, J. H. Heo, T. N. Mandal, S. I. Seok, *Nano Lett.* **2013**, *13*, 1764.
[26] K. Tanaka, T. Takahashi, T. Ban, T. Kondo, K. Uchida, N. Miura, *Solid State Commun.* **2003**, *127*, 619.
[27] N. J. Jeon, J. H. Noh, W. S. Yang, Y. C. Kim, S. Ryu, J. Seo, S. I. Seok, *Nature* **2015**, *517*,476.
[28] Y. Ogomi, A. Morita, S. Tsukamoto, T. Saitho, N. Fujikawa, Q. Shen, T. Toyoda, K. Yoshino, S. S. Pandey, T. Ma, S. Hayase, *J. Phys. Chem. Lett.* **2014**, *5*, 1004.
[29] T. M. Koh, K. Fu, Y. Fang, S. Chen, T. C. Sum, N. Mathews, S. G. Mhaisalkar, P. P. Boix, T. Baikie, *J. Phys. Chem. C* **2014**, *118*, 16458.
[30] T. Umebayashi, K. Asai, T. Kondo, A. Nakao, *Phys. Rev. B* **2003**, *67*, 155405.
[31] A. Amat, E. Mosconi, E. Ronca, C. Quarti, P. Umari, M. K. Nazeeruddin, M. Grätzel, F. De Angelis, *Nano Lett.* **2014**, *14*, 3608.
[32] I. Borriello, G. Cantele, D. Ninno, *Phys. Rev. B* **2008**, *77*, 235214.
[33] T. Baikie, Y. Fang, J. M. Kadro, M. Schreyer, F. Wei, S. G. Mhaisalkar, M. Graetzel, T. J. White, *J. Mater. Chem. A* **2013**, *1*, 5628.
[34] E. Mosconi, P. Umari, F. De Angelis, *J. Mater. Chem. A* **2015**, *3*, 9208.
[35] J. Byun, H. Cho, C. Wolf, M. Jang, A. Sadhanala, R. H. Friend, H. Yang, T.-W. Lee, *Adv. Mater.* **2016**, *28*, 7515.
[36] Y. Bekenstein, B. A. Koscher, S. W. Eaton, P. Yang, A. P. Alivisatos, *J. Am. Chem. Soc.* **2015**, *137*, 16008.
[37] L. Protesescu, S. Yakunin, M. I. Bodnarchuk, F. Krieg, R. Caputo, C. H. Hendon, R. X. Yang, A. Walsh, M. V. Kovalenko, *Nano Lett.* **2015**, *15*, 3692.
[38] M. C. Weidman, M. Seitz, S. D. Stranks, W. A. Tisdale, *ACS Nano* **2016**, *10*, 7830.
[39] Z. Yuan, Y. Shu, Y. Tian, Y. Xin, B. Ma, *Chem. Commun.* **2015**, *51*, 16385.
[40] O. Vybornyi, S. Yakunin, M. V. Kovalenko, *Nanoscale* **2016**, *8*, 6278.
[41] H. Huang, A. S. Susha, S. V. Kershaw, T. F. Hung, A. L. Rogach, *Adv. Sci.* **2015**, *2*, 1500194.
[42] G. Nedelcu, L. Protesescu, S. Yakunin, M. I. Bodnarchuk, M. J. Grotevent, M. V. Kovalenko, *Nano Lett.* **2015**, *15*, 5635.
[43] M. Anaya, A. Rubino, T. C. Rojas, J. F. Galisteo-López, M. E. Calvo, H. Míguez, *Adv. Opt. Mater.* **2017**, *5*, 1601087.
[44] W. van der Stam, J. J. Geuchies, T. Altantzis, K. H. W. van den Bos, J. D. Meeldijk, S. Van Aert, S. Bals, D. Vanmaekelbergh, C. de Mello Donega, *J. Am. Chem. Soc.* **2017**, *139*, 4087.
[45] M. Liu, G. Zhong, Y. Yin, J. Miao, K. Li, C. Wang, X. Xu, C. Shen, H. Meng, *Adv. Sci.* **2017**, *4*, 1700335.
[46] J. A. Sichert, Y. Tong, N. Mutz, M. Vollmer, S. Fischer, K. Z. Milowska, R. García Cortadella, B. Nickel, C. Cardenas-Daw, J. K. Stolarczyk, A. S. Urban, J. Feldmann, *Nano Lett.* **2015**, *15*, 6521.
[47] S. Meloni, T. Moehl, W. Tress, M. Franckevičius, M. Saliba, Y. H. Lee, P. Gao, M. K. Nazeeruddin, S. M. Zakeeruddin, U. Rothlisberger, M. Graetzel, *Nat. Commun.* **2016**, *7*, 10334.
[48] W. Nie, H. Tsai, R. Asadpour, J.-C. Blancon, A. J. Neukirch, G. Gupta, J. J. Crochet, M. Chhowalla, S. Tretiak, M. A. Alam, H.-L. Wang, A. D. Mohite, *Science* **2015**, *347*, 522.
[49] N. Mohammadian, A. Moshaii, A. Alizadeh, S. Gharibzadeh, R. Mohammadpour, *J. Phys. Chem. Lett.* **2016**, *7*, 4614.
[50] J.-P. Correa-Baena, W. Tress, K. Domanski, E. H. Anaraki, S.-H. Turren-Cruz, B. Roose, P. P. Boix, M. Gratzel, M. Saliba, A. Abate, A. Hagfeldt, *Energy Environ. Sci.* **2017**, *10*, 1207.
[51] C. Momblona, L. Gil-Escrig, E. Bandiello, E. M. Hutter, M. Sessolo, K. Lederer, J. Blochwitz-Nimoth, H. J. Bolink, *Energy Environ. Sci.* **2016**, *9*, 3456.
[52] H. Tsai, W. Nie, J.-C. Blancon, C. C. Stoumpos, R. Asadpour, B. Harutyunyan, A. J. Neukirch, R. Verduzco, J. J. Crochet, S. Tretiak, L. Pedesseau, J. Even, M. A. Alam, G. Gupta, J. Lou, P. M. Ajayan, M. J. Bedzyk, M. G. Kanatzidis, A. D. Mohite, *Nature* **2016**, *536*, 312.
[53] P. Vashishtha, J. E. Halpert, *Chem. Mater.* **2017**, *29*, 5965.
[54] J. Wang, N. Wang, Y. Jin, J. Si, Z.-K. Tan, H. Du, L. Cheng, X. Dai, S. Bai, H. He, Z. Ye, M. L. Lai, R. H. Friend, W. Huang, *Adv. Mater.* **2015**, *27*, 2311.
[55] L. Dou, Y. Yang, J. You, Z. Hong, W.-H. Chang, G. Li, Y. Yang, *Nature Commun.* **2014**, *5*, 5404.
[56] X. Y. Chin, D. Cortecchia, J. Yin, A. Bruno, C. Soci, *Nature Commun.* **2015**, *6*,7383.
[57] G. Xing, N. Mathews, S. S. Lim, N. Yantara, X. Liu, D. Sabba, M. Grätzel, S. Mhaisalkar, T. C. Sum, *Nat. Mater.* **2014**, *13*, 476.
[58] K. Chondroudis, D. B. Mitzi, *Chem. Mater.* **1999**, *11*, 3028.
[59] S. Gonzalez-Carrero, R. E. Galian, J. Perez-Prieto, *J. Mater. Chem. A* **2015**, *3*, 9187.
[60] F. Zhang, H. Zhong, C. Chen, X.-G. Wu, X. Hu, H. Huang, J. Han, B. Zou, Y. Dong, *ACS Nano* **2015**, *9*, 4533.
[61] H. Huang, F. Zhao, L. Liu, F. Zhang, X.-G. Wu, L. Shi, B. Zou, Q. Pei, H. Zhong, *ACS Appl. Mater. Interfaces* **2015**, *7*, 28128.
[62] V. Malgras, S. Tominaka, J. W. Ryan, J. Henzie, T. Takei, K. Ohara, Y. Yamauchi, *J. Am. Chem. Soc.* **2016**, *138*, 13874.
[63] V. Amendola, I. Fortunati, C. Marega, A. L. Abdelhady, M. I. Saidaminov, O. M. Bakr, *ChemPhysChem* **2017**, *18*, 1047.
[64] R. Naphade, S. Nagane, G. S. Shanker, R. Fernandes, D. Kothari, Y. Zhou, N. P. Padture, S. Ogale, *ACS Appl. Mater. Interfaces* **2016**, *8*, 854.
[65] L. C. Schmidt, A. Pertegás, S. González-Carrero, O. Malinkiewicz, S. Agouram, G. Mínguez Espallargas, H. J. Bolink, R. E. Galian, J. Pérez-Prieto, *J. Am. Chem. Soc.* **2014**, *136*, 850.
[66] S. Sun, D. Yuan, Y. Xu, A. Wang, Z. Deng, *ACS Nano* **2016**, *10*, 3648.
[67] S. Demchyshyn, J. M. Roemer, H. Groiß, H. Heilbrunner, C. Ulbricht, D. Apaydin, A. Böhm, U. Rütt, F. Bertram, G. Hesser, M. C. Scharber, N. S. Sariciftci, B. Nickel, S. Bauer, E. D. Głowacki, M. Kaltenbrunner, *Sci. Adv.* **2017**, *3*, e1700738.
[68] S. Bhaumik, S. A. Veldhuis, Y. F. Ng, M. Li, S. K. Muduli, T. C. Sum, B. Damodaran, S. Mhaisalkar, N. Mathews, *Chem. Commun.* **2016**, *52*, 7118.
[69] B. Luo, Y.-C. Pu, Y. Yang, S. A. Lindley, G. Abdelmageed, H. Ashry, Y. Li, X. Li, J. Z. Zhang, *J. Phys. Chem. C* **2015**, *119*, 26672.
[70] P. Tyagi, S. M. Arveson, W. A. Tisdale, *J. Phys. Chem. Lett.* **2015**, *6*, 1911.
[71] S. Pathak, N. Sakai, F. Wisnivesky Rocca Rivarola, S. D. Stranks, J. Liu, G. E. Eperon, C. Ducati, K. Wojciechowski, J. T. Griffiths, A. A. Haghighirad, A. Pellaroque, R. H. Friend, H. J. Snaith, *Chem. Mater.* **2015**, *27*, 8066.
[72] Y. Hassan, Y. Song, R. D. Pensack, A. I. Abdelrahman, Y. Kobayashi, M. A. Winnik, G. D. Scholes, *Adv. Mater.* **2016**, *28*, 566.
[73] F. Liu, Y. Zhang, C. Ding, S. Kobayashi, T. Izuishi, N. Nakazawa, T. Toyoda, T. Ohta, S. Hayase, T. Minemoto, K. Yoshino, S. Dai, Q. Shen, *ACS Nano* **2017**, *11*, 10373.
[74] K. Akihiro, I. Masashi, T. Kenjiro, M. Tsutomu, *Chem. Lett.* **2012**, *41*, 397.
[75] M. Kulbak, S. Gupta, N. Kedem, I. Levine, T. Bendikov, G. Hodes, D. Cahen, *J. Phys. Chem. Lett.* **2016**, *7*, 167.

[76] B. Conings, J. Drijkoningen, N. Gauquelin, A. Babayigit, J. D'Haen, L. D'Olieslaeger, A. Ethirajan, J. Verbeeck, J. Manca, E. Mosconi, F. D. Angelis, H.-G. Boyen, *Adv. Energy Mater.* **2015**, *5*, 1500477.

[77] D. Zhang, S. W. Eaton, Y. Yu, L. Dou, P. Yang, *J. Am. Chem. Soc.* **2015**, *137*, 9230.

[78] A. Pan, B. He, X. Fan, Z. Liu, J. J. Urban, A. P. Alivisatos, L. He, Y. Liu, *ACS Nano* **2016**, *10*, 7943.

[79] I. Lignos, S. Stavrakis, G. Nedelcu, L. Protesescu, A. J. deMello, M. V. Kovalenko, *Nano Lett.* **2016**, *16*, 1869.

[80] Q. A. Akkerman, S. G. Motti, A. R. Srimath Kandada, E. Mosconi, V. D'Innocenzo, G. Bertoni, S. Marras, B. A. Kamino, L. Miranda, F. De Angelis, A. Petrozza, M. Prato, L. Manna, *J. Am. Chem. Soc.* **2016**, *138*, 1010.

[81] J. Shamsi, Z. Dang, P. Bianchini, C. Canale, F. Di Stasio, R. Brescia, M. Prato, L. Manna, *J. Am. Chem. Soc.* **2016**, *138*, 7240.

[82] D. Amgar, A. Stern, D. Rotem, D. Porath, L. Etgar, *Nano Lett.* **2017**, *17*, 1007.

[83] T. C. Jellicoe, J. M. Richter, H. F. J. Glass, M. Tabachnyk, R. Brady, S. E. Dutton, A. Rao, R. H. Friend, D. Credgington, N. C. Greenham, M. L. Böhm, *J. Am. Chem. Soc.* **2016**, *138*, 2941.

[84] Y. Tong, E. Bladt, M. F. Aygüler, A. Manzi, K. Z. Milowska, V. A. Hintermayr, P. Docampo, S. Bals, A. S. Urban, L. Polavarapu, J. Feldmann, *Angew. Chem., Int. Ed.* **2016**, *55*, 13887.

[85] Z.-Y. Zhu, Q.-Q. Yang, L.-F. Gao, L. Zhang, A.-Y. Shi, C.-L. Sun, Q. Wang, H.-L. Zhang, *J. Phys. Chem. Lett.* **2017**, *8*, 1610.

[86] F. Zhu, L. Men, Y. Guo, Q. Zhu, U. Bhattacharjee, P. M. Goodwin, J. W. Petrich, E. A. Smith, J. Vela, *ACS Nano* **2015**, *9*, 2948.

[87] P. Zhu, S. Gu, X. Shen, N. Xu, Y. Tan, S. Zhuang, Y. Deng, Z. Lu, Z. Wang, J. Zhu, *Nano Lett.* **2016**, *16*, 871.

[88] J. Xing, X. F. Liu, Q. Zhang, S. T. Ha, Y. W. Yuan, C. Shen, T. C. Sum, Q. Xiong, *Nano Lett.* **2015**, *15*, 4571.

[89] M. Spina, E. Bonvin, A. Sienkiewicz, B. Náfrádi, L. Forró, E. Horváth, *Scientific Reports* **2016**, *6*, 19834.

[90] L. Dou, A. B. Wong, Y. Yu, M. Lai, N. Kornienko, S. W. Eaton, A. Fu, C. G. Bischak, J. Ma, T. Ding, N. S. Ginsberg, L.-W. Wang, A. P. Alivisatos, P. Yang, *Science* **2015**, *349*, 1518.

[91] V. A. Hintermayr, A. F. Richter, F. Ehrat, M. Döblinger, W. Vanderlinden, J. A. Sichert, Y. Tong, L. Polavarapu, J. Feldmann, A. S. Urban, *Adv. Mater.* **2016**, *28*, 9478.

[92] W. Deng, X. Xu, X. Zhang, Y. Zhang, X. Jin, L. Wang, S.-T. Lee, J. Jie, *Adv. Funct. Mater.* **2016**, *26*, 4797.

[93] A. Perumal, S. Shendre, M. Li, Y. K. E. Tay, V. K. Sharma, S. Chen, Z. Wei, Q. Liu, Y. Gao, P. J. S. Buenconsejo, S. T. Tan, C. L. Gan, Q. Xiong, T. C. Sum, H. V. Demir, *Sci. Rep.* **2016**, *6*, 36733.

[94] J. Song, J. Li, X. Li, L. Xu, Y. Dong, H. Zeng, *Adv. Mater.* **2015**, *27*, 7162.

[95] X. Tang, Z. Hu, W. Chen, X. Xing, Z. Zang, W. Hu, J. Qiu, J. Du, Y. Leng, X. Jiang, L. Mai, *Nano Energy* **2016**, *28*, 462.

[96] X. Zhang, H. Lin, H. Huang, C. Reckmeier, Y. Zhang, W. C. H. Choy, A. L. Rogach, *Nano Lett.* **2016**, *16*, 1415.

[97] G. Li, F. W. R. Rivarola, N. J. L. K. Davis, S. Bai, T. C. Jellicoe, F. de la Peña, S. Hou, C. Ducati, F. Gao, R. H. Friend, N. C. Greenham, Z.-K. Tan, *Adv. Mater.* **2016**, *28*, 3528.

[98] J. Li, L. Xu, T. Wang, J. Song, J. Chen, J. Xue, Y. Dong, B. Cai, Q. Shan, B. Han, H. Zeng, *Adv. Mater.* **2017**, *29*, 1603885.

[99] X. Y. Chin, A. Perumal, A. Bruno, N. Yantara, S. A. Veldhuis, L. Martínez-Sarti, B. Chandran, V. Chirvony, A. S.-Z. Lo, J. So, C. Soci, M. Grätzel, H. J. Bolink, N. Mathews, S. G. Mhaisalkar, *Energy Environ. Sci.* **2018**, *11*, 1770.

[100] M. Era, S. Morimoto, T. Tsutsui, S. Saito, *Appl. Phys. Lett.* **1994**, *65*, 676.

[101] T. Hattori, T. Taira, M. Era, T. Tsutsui, S. Saito, *Chem. Phys. Lett.* **1996**, *254*, 103.

[102] N. K. Kumawat, A. Dey, A. Kumar, S. P. Gopinathan, K. L. Narasimhan, D. Kabra, *ACS Appl. Mater. Interfaces* **2015**, *7*, 13119.

[103] D. Bi, W. Tress, M. I. Dar, P. Gao, J. Luo, C. Renevier, K. Schenk, A. Abate, F. Giordano, J.-P. Correa Baena, J.-D. Decoppet, S. M. Zakeeruddin, M. K. Nazeeruddin, M. Grätzel, A. Hagfeldt, *Sci. Adv.* **2016**, *2*, e1501170.

[104] H. P. Kim, J. Kim, B. S. Kim, H.-M. Kim, J. Kim, A. R. B. M. Yusoff, J. Jang, M. K. Nazeeruddin, *Adv. Opt. Mater.* **2017**, *5*, 1600920.

[105] N. Yantara, S. Bhaumik, F. Yan, D. Sabba, H. A. Dewi, N. Mathews, P. P. Boix, H. V. Demir, S. Mhaisalkar, *J. Phys. Chem. Lett.* **2015**, *6*, 4360.

[106] L. Song, X. Guo, Y. Hu, Y. Lv, J. Lin, Z. Liu, Y. Fan, X. Liu, *J. Phys. Chem. Lett.* **2017**, *8*, 4148.

[107] M. Saba, M. Cadelano, D. Marongiu, F. Chen, V. Sarritzu, N. Sestu, C. Figus, M. Aresti, R. Piras, A. Geddo Lehmann, C. Cannas, A. Musinu, F. Quochi, A. Mura, G. Bongiovanni, *Nat. Commun.* **2014**, *5*, 5049.

[108] S. D. Stranks, V. M. Burlakov, T. Leijtens, J. M. Ball, A. Goriely, H. J. Snaith, *Phys. Rev. Appl.* **2014**, *2*, 034007.

[109] X. Wu, M. T. Trinh, D. Niesner, H. Zhu, Z. Norman, J. S. Owen, O. Yaffe, B. J. Kudisch, X. Y. Zhu, *J. Am. Chem. Soc.* **2015**, *137*, 2089.

[110] T. J. Savenije, C. S. Ponseca, L. Kunneman, M. Abdellah, K. Zheng, Y. Tian, Q. Zhu, S. E. Canton, I. G. Scheblykin, T. Pullerits, A. Yartsev, V. Sundström, *J. Phys. Chem. Lett.* **2014**, *5*, 2189.

[111] C. Wehrenfennig, G. E. Eperon, M. B. Johnston, H. J. Snaith, L. M. Herz, *Adv. Mater.* **2014**, *26*, 1584.

[112] R. Sheng, A. Ho-Baillie, S. Huang, S. Chen, X. Wen, X. Hao, M. A. Green, *J. Phys. Chem. C* **2015**, *119*, 3545.

[113] Z. Xiao, R. A. Kerner, L. Zhao, N. L. Tran, K. M. Lee, T.-W. Koh, G. D. Scholes, B. P. Rand, *Nat. Photonics* **2017**, *11*, 108.

[114] Y. F. Ng, S. A. Kulkarni, S. Parida, N. F. Jamaludin, N. Yantara, A. Bruno, C. Soci, S. Mhaisalkar, N. Mathews, *Chem. Commun.* **2017**, *53*, 12004.

[115] L. Zhao, Y.-W. Yeh, N. L. Tran, F. Wu, Z. Xiao, R. A. Kerner, Y. L. Lin, G. D. Scholes, N. Yao, B. P. Rand, *ACS Nano* **2017**, *11*, 3957.

[116] J.-W. Lee, Y. J. Choi, J.-M. Yang, S. Ham, S. K. Jeon, J. Y. Lee, Y.-H. Song, E. K. Ji, D.-H. Yoon, S. Seo, H. Shin, G. S. Han, H. S. Jung, D. Kim, N.-G. Park, *ACS Nano* **2017**, *11*, 3311.

[117] N. Ahn, D.-Y. Son, I.-H. Jang, S. M. Kang, M. Choi, N.-G. Park, *J. Am. Chem. Soc.* **2015**, *137*, 8696.

[118] S. A. Kulkarni, S. Muduli, G. Xing, N. Yantara, M. Li, S. Chen, T. C. Sum, N. Mathews, T. J. White, S. G. Mhaisalkar, *ChemSusChem* **2017**, *10*, 3818.

[119] M. F. Aygüler, M. D. Weber, B. M. D. Puscher, D. D. Medina, P. Docampo, R. D. Costa, *J. Phys. Chem. C* **2015**, *119*, 12047.

[120] Y. Ling, Z. Yuan, Y. Tian, X. Wang, J. C. Wang, Y. Xin, K. Hanson, B. Ma, H. Gao, *Adv. Mater.* **2016**, *28*, 305.

[121] S. Kumar, J. Jagielski, S. Yakunin, P. Rice, Y.-C. Chiu, M. Wang, G. Nedelcu, Y. Kim, S. Lin, E. J. G. Santos, M. V. Kovalenko, C.-J. Shih, *ACS Nano* **2016**, *10*, 9720.

[122] M. B. Johnston, L. M. Herz, *Acc. Chem. Res.* **2016**, *49*, 146.

[123] G. Xing, B. Wu, X. Wu, M. Li, B. Du, Q. Wei, J. Guo, E. K. L. Yeow, T. C. Sum, W. Huang, *Nat. Commun.* **2017**, *8*, 14558.

[124] A. Kurzmann, A. Ludwig, A. D. Wieck, A. Lorke, M. Geller, *Nano Lett.* **2016**, *16*, 3367.

[125] F. Deschler, M. Price, S. Pathak, L. E. Klintberg, D.-D. Jarausch, R. Higler, S. Hüttner, T. Leijtens, S. D. Stranks, H. J. Snaith, M. Atatüre, R. T. Phillips, R. H. Friend, *J. Phys. Chem. Lett.* **2014**, *5*, 1421.

[126] H. Zhu, Y. Fu, F. Meng, X. Wu, Z. Gong, Q. Ding, M. V. Gustafsson, M. T. Trinh, S. Jin, X. Y. Zhu, *Nat. Mater.* **2015**, *14*, 636.

[127] O. D. Miller, E. Yablonovitch, S. R. Kurtz, *IEEE J. Photovoltaics* **2012**, *2*, 303.

[128] A. Swarnkar, A. R. Marshall, E. M. Sanehira, B. D. Chernomordik, D. T. Moore, J. A. Christians, T. Chakrabarti, J. M. Luther, *Science* **2016**, *354*, 92.

[129] L. M. Pazos-Outón, M. Szumilo, R. Lamboll, J. M. Richter, M. Crespo-Quesada, M. Abdi-Jalebi, H. J. Beeson, M. Vrućinić,

M. Alsari, H. J. Snaith, B. Ehrler, R. H. Friend, F. Deschler, *Science* **2016**, *351*, 1430.
[130] E. M. Sanehira, A. R. Marshall, J. A. Christians, S. P. Harvey, P. N. Ciesielski, L. M. Wheeler, P. Schulz, L. Y. Lin, M. C. Beard, J. M. Luther, *Sci. Adv.* **2017**, *3*, eaao4204.
[131] M. Li, S. Bhaumik, T. W. Goh, M. S. Kumar, N. Yantara, M. Grätzel, S. Mhaisalkar, N. Mathews, T. C. Sum, *Nat. Commun.* **2017**, *8*, 14350.
[132] Z. Guo, Y. Wan, M. Yang, J. Snaider, K. Zhu, L. Huang, *Science* **2017**, *356*, 59.
[133] X. Zhang, G. Wu, S. Yang, W. Fu, Z. Zhang, C. Chen, W. Liu, J. Yan, W. Yang, H. Chen, *Small* **2017**, *13*, 1700611.
[134] G. Grancini, C. Roldán-Carmona, I. Zimmermann, E. Mosconi, X. Lee, D. Martineau, S. Narbey, F. Oswald, F. De Angelis, M. Graetzel, M. K. Nazeeruddin, *Nat. Commun.* **2017**, *8*, 15684.
[135] C. C. Stoumpos, D. H. Cao, D. J. Clark, J. Young, J. M. Rondinelli, J. I. Jang, J. T. Hupp, M. G. Kanatzidis, *Chem. Mater.* **2016**, *28*, 2852.
[136] Z. Wang, Q. Lin, F. P. Chmiel, N. Sakai, L. M. Herz, H. J. Snaith, *Nat. Energy* **2017**, *2*, 17135.
[137] M. Auf der Maur, A. Pecchia, G. Penazzi, W. Rodrigues, A. Di Carlo, *Phys. Rev. Lett.* **2016**, *116*, 027401.
[138] D. H. Cao, C. C. Stoumpos, T. Yokoyama, J. L. Logsdon, T.-B. Song, O. K. Farha, M. R. Wasielewski, J. T. Hupp, M. G. Kanatzidis, *ACS Energy Lett.* **2017**, *2*, 982.
[139] W. S. A. H. J. Queisser, *J. Appl. Phys.* **1961**, *32*, 1776.
[140] A. J. Nozik, *Annu. Rev. Phys. Chem.* **2001**, *52*, 193.
[141] M. A. Green, *Prog. Photovoltaics* **2001**, *9*, 123.
[142] D. König, K. Casalenuovo, Y. Takeda, G. Conibeer, J. F. Guillemoles, R. Patterson, L. M. Huang, M. A. Green, *Phys. E* **2010**, *42*, 2862.
[143] B. N. Murdin, W. Heiss, C. J. G. M. Langerak, S. C. Lee, I. Galbraith, G. Strasser, E. Gornik, M. Helm, C. R. Pidgeon, *Phys. Rev. B* **1997**, *55*, 5171.
[144] W. Pötz, *Phys. Rev. B* **1987**, *36*, 5016.
[145] Q. Shen, T. S. Ripolles, J. Even, Y. Ogomi, K. Nishinaka, T. Izuishi, N. Nakazawa, Y. Zhang, C. Ding, F. Liu, T. Toyoda, K. Yoshino, T. Minemoto, K. Katayama, S. Hayase, *Appl. Phys. Lett.* **2017**, *111*, 153903.
[146] J. Yang, X. Wen, H. Xia, R. Sheng, Q. Ma, J. Kim, P. Tapping, T. Harada, T. W. Kee, F. Huang, Y.-B. Cheng, M. Green, A. Ho-Baillie, S. Huang, S. Shrestha, R. Patterson, G. Conibeer, *Nat. Commun.* **2017**, *8*, 14120.
[147] Y. Yang, D. P. Ostrowski, R. M. France, K. Zhu, J. van de Lagemaat, J. M. Luther, M. C. Beard, *Nat. Photonics* **2016**, *10*, 53.
[148] H. Zhu, K. Miyata, Y. Fu, J. Wang, P. P. Joshi, D. Niesner, K. W. Williams, S. Jin, X.-Y. Zhu, *Science* **2016**, *353*, 1409.
[149] M. E. Madjet, G. R. Berdiyorov, F. El-Mellouhi, F. H. Alharbi, A. V. Akimov, S. Kais, *J. Phys. Chem. Lett.* **2017**, *8*, 4439.
[150] G. Conibeer, S. Shrestha, S. Huang, R. Patterson, H. Xia, Y. Feng, P. Zhang, N. Gupta, M. Tayebjee, S. Smyth, Y. Liao, S. Lin, P. Wang, X. Dai, S. Chung, *Sol. Energy Mater. Sol. Cells* **2015**, *135*, 124.
[151] P. Papagiorgis, L. Protesescu, M. V. Kovalenko, A. Othonos, G. Itskos, *J. Phys. Chem. C* **2017**, *121*, 12434.
[152] Q. A. Akkerman, V. D'Innocenzo, S. Accornero, A. Scarpellini, A. Petrozza, M. Prato, L. Manna, *J. Am. Chem. Soc.* **2015**, *137*, 10276.
[153] R. Yan, D. Gargas, P. Yang, *Nat. Photonics* **2009**, *3*, 569.
[154] R. Chen, T.-T. D. Tran, K. W. Ng, W. S. Ko, L. C. Chuang, F. G. Sedgwick, C. Chang-Hasnain, *Nat. Photonics* **2011**, *5*, 170.
[155] F. Qian, Y. Li, S. Gradečak, H.-G. Park, Y. Dong, Y. Ding, Z. L. Wang, C. M. Lieber, *Nat. Mater.* **2008**, *7*, 701.
[156] D. Saxena, S. Mokkapati, P. Parkinson, N. Jiang, Q. Gao, H. H. Tan, C. Jagadish, *Nat. Photonics* **2013**, *7*, 963.
[157] S. W. Eaton, M. Lai, N. A. Gibson, A. B. Wong, L. Dou, J. Ma, L.-W. Wang, S. R. Leone, P. Yang, *Proc. Natl. Acad. Sci. USA* **2016**, *113*, 1993.